J. Chem. Soc. Nigeria, Vol. 50, No. 1, pp 101 – 139 [2025]

MAJOR, TRACE, AND RARE EARTH ELEMENTS GEOCHEMISTRY OF THE LATE PALEOCENE SHALES FROM GAMBA FORMATION, SOKOTO BASIN, NORTHWEST NIGERIA

A.B. Ogbesejana[1*], L. A. Muaz[1], N.S. Gobirawa[1], F.D. Radda[1], S.A. Akinyemi[2], A.M. Adeleye[3], A.C. Egwu[4], B.M. Sarki Yandoka[5].

[1]Department of Industrial Chemistry, Faculty of Physical Sciences, Federal University Dutsin-Ma, P.M.B. 5001, Katsina State, Nigeria.
[2]Department of Geology, Faculty of Science, Ekiti State University, P.M.B., 5363, Ado Ekiti, Ekiti State, Nigeria.
[3]Department of Chemistry, University of Ibadan, Oyo State, Nigeria.
[4]BGI Laboratory Limited, 278 Port-Harcourt/Aba Expressway, Port-Harcourt, Rivers State, Nigeria.
[5]Department of Geology, Bayero University, P.M.B. 3011, Kano State, Nigeria.
Correspondence email: abiodunogbesejana@gmail.com

ABSTRACT

The present investigation delved into the geochemical importance of trace elements and major oxide constituents in the shales from the Gamba Formation, Sokoto Basin, Nigeria. by inductively coupled plasma-mass spectrometry (ICP-MS), x-ray fluorescence spectroscopy (XRF), and statistical methodologies within the context of provenance, tectonic environments, and conditions of deposition. Alkali metals and alkali-earth metal elements, Na, K, Ca, and Mg occurred in very high concentrations in the shale samples while U has the lowest values, indicating the detritus derived from various provenances (felsic and mafic) and reducing conditions of the environment. Among the rare earth elements detected in the shales, light rare earth elements showed enriched concentrations compared to heavy rare earth elements, indicating anoxic conditions. Among the major oxides identified, the shales exhibit elevated levels of SiO_2, with Fe_2O_3 greater than Al_2O_3; whereas the remaining oxides demonstrate relatively low concentrations. This suggests that shales are predominantly constituted of quartz minerals and were formed in marine settings. Moreover, the distribution patterns of the trace elements and major oxides showed striking similarities in the spider diagrams of UCC and PAAS. The ratios derived from both the trace elements and major oxides, along with the discrimination diagrams, indicated that the shales consist of mafic and felsic detritus. They were likely deposited under varying conditions, such as anoxic and oxic, near the passive margin and continental island arc. These conclusions were further corroborated by the multivariate statistical analyses conducted on the elemental dataset. This study demonstrated the effectiveness of trace elements and major oxides geochemistry in assessing the origin, tectonic setting, and paleoenvironments of shales.

Keywords: Shales, trace elements, major oxides, ICP-MS, XRF, Sokoto basin.

INTRODUCTION

The elemental compositions of shales, including major, trace, and rare earth elements, are commonly utilized for indicating the origin, past climate, weathering conditions, tectonic environment,

ISSN 0795 - 22066

rate of primary productivity, and environmental changes in the past [1, 2, 3, 4, 5, 6, 7, 8, 9, 10, 11, 12, 13, 14]. Geochemical compositions are particularly valuable for elucidating the weathering and sorting chronicles of siltstones, mudstones, and shales due to their exceedingly fine and uniform grain size, which impedes the reflection of such geochemical data. The correlation between major oxides found in sediments and their origin is not entirely consistent with that of their source rocks due to compositional fractionation resulting from varying weathering processes within different tectonic environments [12,13,15].

The Al_2O_3/TiO_2 ratios and Al/Ti ratios of sediments tend to mirror those of their parent rocks, while elements such as Na, K, Ca, Mg, Fe, and Mn may undergo partial or complete loss through erosion, transportation, and sediment deposition [2, 4, 16]. Hence, primary oxides are predominantly utilized for interpreting the process of weathering in detritus, understanding past climates, and reconstructing tectonic environments [7, 17, 18] Trace elements and rare earth elements (REEs) that are immobile exhibit resistance to chemical weathering, resulting in lesser leaching compared to major oxides during the erosion and weathering of sediments [5, 16, 19]. The elemental ratios such as Cr/Th, La/Th, Co/Th, La/Sc, and Th/Sc are commonly employed to indicate the origin of sedimentary rocks [3, 5, 10, 11, 20]. Hence, the analysis of trace elements and rare earth elements (REEs) is conducted extensively to differentiate detritus origin and tectonic context [5, 7, 8, 10, 11, 21, 22, 23].

Numerous investigations have been conducted within the Sokoto basin, as documented by Kogbe [24, 25, 26], Obaje [27, 28], Obaje *et al*. [29, 30], Toyin *et al*. [31], and Emujakporue *et al*. [32]. Toyin *et al*. [31,33] have presented findings concerning the lithostratigraphic, paleontological, and sedimentological attributes, along with the reservoir potential, of carbonate fomations originating from different sectors of this particular basin. It is noteworthy to highlight that Kogbe [24, 26] and Reyment [34] have formerly outlined the overall geological characteristics of the broader Iullemmeden basin. Moreover, the endeavor of the Nigerian government to explore hydrocarbon resources in the inland basins of Nigeria has stimulated the investigation conducted by Obaje *et al*. [29]. Nevertheless, the focal point of a large portion of these investigations has been on subjects like regional geology, stratigraphic sequence, sedimentology, geological mapping, and aeromagnetic geophysical exploration.

ISSN 0795 - 22066

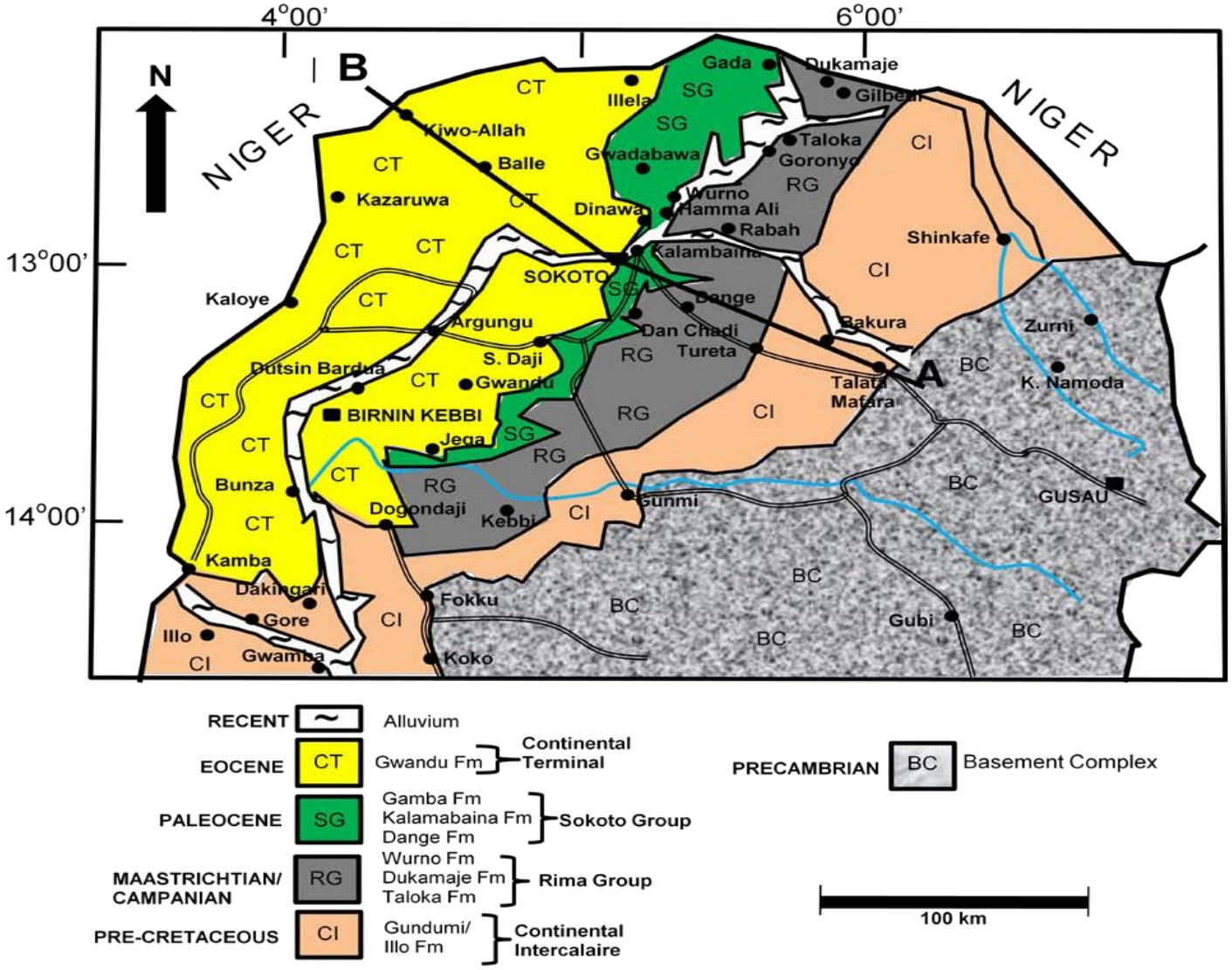

Fig. 1: Generalized geological map of the Nigerian sector of lullemmeden Basin (Sokoto Basin) showing the study locations (adopted from [29]).

However, these investigations did not provide an adequate understanding of the shale's petroleum-generative capacity within the basin, a critical aspect of petroleum exploration. To date, research on the origin, ancient environment, and tectonic context of the shales in the Sokoto Basin through elemental indicators remains notably insufficient [9, 35, 36]. Bassey and Eminue [35] applied

ISSN 0795 - 22066

atomic absorption spectrometry (AAS) and x-ray fluorescence spectrometry (XRF) to study the shales from Dukumaje and Taloka formations and concluded that the shales from these formations were deposited exclusively from marine environments with mixed provenance (mafic and felsic). Boboye *et al.* [36] applied inductively coupled plasma-emission spectrometry (ICP-ES) and inductively coupled plasma-mass spectrometry (ICP-MS) to three Nigerian inland Basins (Chad, Dahomey, and Sokoto) with only one sample from Dange formation in the Sokoto Basin and concluded that this sample was deposited under marine environments with igneous rock compositions. Additionally, the study of Toyin *et al*. [9] focused on the shales from the Dange formation where it concluded that Dange shales have a mafic–intermediate source and island arc–active continental margin province. To the best of our knowledge, the detailed elemental geochemistry of the shales from the Gamba formation has not been reported. Hence, samples were gathered to examine the origin, assess the sedimentary environment, and distinguish the tectonic context of the shales within the Gamba formation. The objective is to enhance the understanding of the origin, paleoenvironments, and tectonic history related to the development of the shales within the Sokoto basin in the Late Paleocene epoch. This could offer valuable insights for the exploration of shale oil and gas resources in this region.

GEOLOGICAL AND STRATIGRAPHIC SETTINGS OF SOKOTO BASIN

The Sokoto Basin, situated in northwestern Nigeria, constitutes the southeastern sector of the broader Iullemmeden basin (Fig. 1). Within the Iullemmeden basin, encompassing regions of Niger Republic, Benin, Mali, Algeria, and Libya, the major depocenters are predominantly located in Niger [26]. In terms of stratigraphy, the Nigerian sector reflects the exposed basin margin of the Iullemmeden basin, characterized by a reduction in sediment thickness and stratigraphic age moving from Niger, where it is thickest and oldest, towards Nigeria. It is further postulated that an influx of oceanic water penetrated the Sokoto basin from the Tethys Sea, ultimately connecting to the southern Atlantic [26]. Primarily, the Sokoto Basin represents a gently rolling plain with an average altitude ranging from 250 to 400 meters above sea level. This expanse is sporadically punctuated by small plateaus. The "Dange Scarp" constitutes a minor cliff and stands out as the most prominent characteristic in the basin. The Gundumi Formation situated in the northeast and the Illo Formation located in the southwest are identified as the "Continental Intercalary" Group [24, 25, 37, 38]. These two formations

ISSN 0795 - 22066

represent lateral equivalents, with a sediment thickness reaching up to 300 meters.

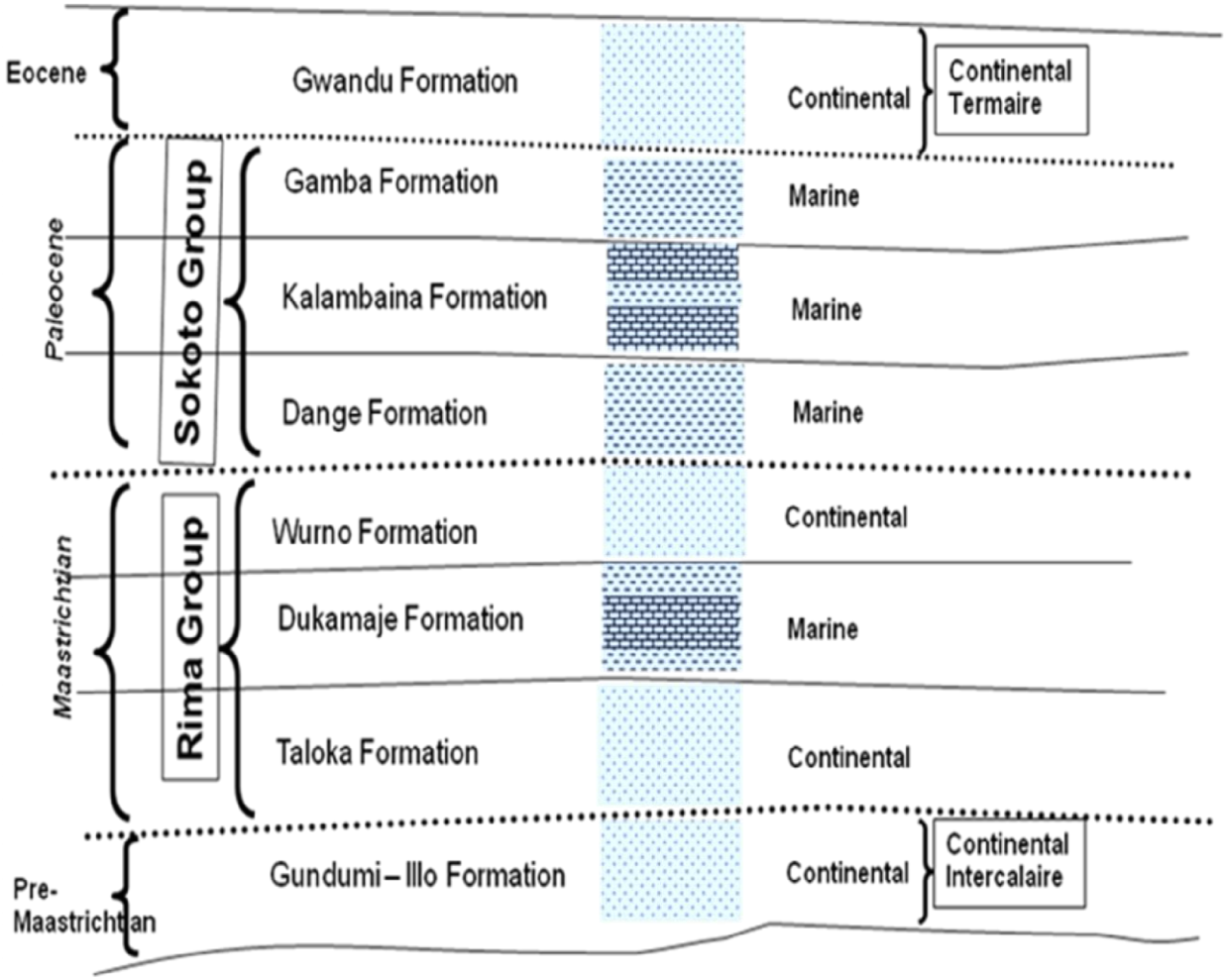

Fig. 2: Stratigraphic successions in the Nigerian sector of lullemmeden Basin (Sokoto Basin) adopted from [29].

The Illo-Gundumi sequence is composed of a lower section characterized by white conglomeratic, arkosic, cross-bedded sandstones containing interbedded concretionary and highly aluminous clays, and an upper section comprising coarse to medium, cross-bedded sandstones. Overlying these Formations in an unconformable manner is the Maastrichtian Rima Group, which includes the Taloka, Dukamaje, and Wurno Formations. The Taloka Formation has a thickness of 50 meters, transitioning into a clayey composition towards the top. At this stratigraphic level, there is a transition to a 10-meter-thick layer of gypsum-bearing, fissile, bluish-grey shale containing marl within the Dukamaje Formation. The

ISSN 0795 - 22066

foraminiferal microfaunas found in the Dukamaje Formation indicate an age range from the Middle to Late Maastrichtian period [39, 40]. While marine Maastrichtian deposits are present in the Iullemmeden basin, both exposed and subsurface, in Mali and Niger [41, 42, 43, 44], they gradually thin out towards the northwest of Sokoto in the southeastern region of the Iullemmeden basin. The Sokoto Group is categorized into three main divisions: Firstly, the lower Dange Formation comprises 10m gypsiferous, greenish-grey paper shale that contains abundant Paleocene vertebrates and arenaceous foraminifera. Secondly, the middle Kalambaina Formation is characterized by a 10-m fossiliferous marly limestone hosting shallow, warm-water Tethyan Late Paleocene benthonic foraminifera. Lastly, the upper 2-m greenish-grey paper shale situated at the summit of the Kalambaina Formation exhibits an impoverished arenaceous foraminiferal assemblage. The Gamba Formation, as identified by Kogbe [45], is denoted as the latter unit. Within the northwestern region of Nigeria, the Gwandu Formation or the "Continental Terminal" Group (referred to in francophone West Africa) is characterized by continental deposits that disconformably rest above the Upper Paleocene marine strata situated in the southeastern Iullemmeden basin. These Tertiary lacustrine clays, cross-bedded sandstones, and siltstones exhibit variegation and are observed as mesas in the Iullemmeden basin, with thicknesses reaching up to 300 m at the basin's core. The geological illustration delineating the rock sequence throughout the extensive Iullemmeden basin can be observed in Figure 2.

MATERIALS AND METHODS

SAMPLING

A total of twenty (20) outcrop shale samples were collected from the Gamba Formation in the Sokoto Basin, Northwestern Nigeria. The geological map and stratigraphic sequence are shown in Figures 1 and 2.

SAMPLE PREPARATION

All glassware utilized in the experiment underwent thorough washing and rinsing with distilled water. They were then immersed in a chromic acid solution for 24 hours. Subsequently, the specimens underwent a thorough rinsing process using deionized distilled water, followed by drying in an oven set at a temperature of 110˚C. Ultimately, the specimens were transferred to desiccators for cooling purposes. The samples were then processed through grinding using an agate

ISSN 0795 - 22066

mortar. The resultant pounded samples were individually sifted through a 100um-mesh size sieve. To avoid cross-contamination, the pestle and mortar were meticulously cleaned following the grinding of each sample.

INDUCTIVELY COUPLED PLASMA-MASS SPECTROMETRY (ICP-MS) ANALYSIS

The shale samples were analyzed at BGI laboratory services, Port-Harcourt, Rivers State, Nigeria, after being subjected to a digestion procedure employing a concentrated sulfuric acid and a 30% solution of hydrogen peroxide. To extract the water-soluble salts of metals from the shales, a volume of three milliliters of deionized water was added to 2.0 grams of each shale sample and vigorously shaken. The adequate separation of the two phases was successfully attained via centrifugation of the specimens. Subsequently, the organic phase (shale) was subjected to digestion using 3 milliliters of concentrated H_2SO_4, inducing the carbonization of the specimen to ensure thorough decomposition. This was then followed by the introduction of 4 milliliters of 30% hydrogen peroxide for oxidation. The produced aqueous solution was diluted to a volume of 10 milliliters using deionized water and demonstrated a colorless appearance suitable for standard ICP-MS analysis. Following this, a multi-element standard solution was formulated by diluting stock solutions of the elements with deionized distilled water to create individual working solutions for calibration purposes. The elemental findings are detailed in Table 1.

X-RAY FLUORESCENCE SPECTROMETRY (XRF) ANALYSIS

4g rock powders with a grain size of approximately 300 meshes underwent compression to form a pellet inside a disk measuring 32mm in diameter at a pressure of 32MPa. Subsequently, the pellets were analyzed at the analytical laboratory, Department of Chemistry, Umaru Musa University, Katsina State, Nigeria using an Axios 4.0 X-ray fluorescence spectrometer. The operational parameters for the XRF machine included V=60kV, I=120mA, and P=4kW. To ensure the accuracy of major oxide measurements, the average precision was maintained at below 2%. The results of major oxides are presented in Table 2.

ISSN 0795 - 22066

Table 1: The concentrations (ppm) of the elements in the shales from Gamba formation.

Sample (ppm)	Ba	Bi	Ca	Ce	Eu	Gd	Hf	K	Mg	Na	Tb	Nb	Pr	Sm	Sr	Ta	Th	Ti	U	Zn
GB 01	7.4	4.4	2220.6	0.46	0.66	6.4	0.74	996.6	817.84	197.82	3.2	0.68	5	6.4	5.2	0.9	6.2	4.4	2	6.8
GB 02	9.8	4.2	2202.2	0.66	0.88	7.2	0.52	1002	1022	199.84	2.4	1.8	6.4	4.6	6.6	0.66	6.8	6.8	2.4	6.6
GB 03	13.4	5.6	1826.4	0.78	0.52	7.4	0.9	1000.4	934.42	452.64	3	1.28	7.2	6.4	5.6	0.8	14.22	6.8	2.4	8
GB 04	17.6	6.4	2354	0.7	1.08	11	0.38	1202.2	1032.2	687.18	3.8	1.1	11.6	4.8	5.2	1.62	2.42	7.2	1.8	6.8
GB 05	11	6.6	2844.6	0.56	0.46	9.6	0.22	799.8	992.44	653.44	3.6	1.24	6.8	6.4	6.4	0.64	5.24	11	0.2	3
GB 06	4.6	6.8	2206.2	0.66	0.64	4.6	0.38	1131.2	1224.54	199.66	5.2	0.68	6.4	7	5.2	0.76	18	7.8	0.8	2.6
GB 07	4.2	6.4	177.6	0.92	0.9	3.4	0.44	1022.2	1008.44	575.78	3.2	0.88	4.6	5.2	5.8	0.22	6.68	6	0.8	4
GB 08	6.8	8.4	1832.6	0.98	0.82	4.4	0.7	1332	975.84	730.6	3.2	0.94	7.8	4.8	4.4	0.4	10.42	6.8	0.6	4.2
GB 09	4.8	6	1976	0.64	0.56	6.6	0.38	704.2	997.44	606.44	3.8	1.12	4.4	3	4.6	1.6	9.3	5	1	4
GB 10	2.6	6.8	1999.8	0.78	0.48	5	0.42	1086.6	1026.84	732.66	2.8	1.6	7.6	5.2	5.8	1.12	15.32	6	0.8	4.2
GB 11	9	7	1022.8	0.68	0.46	2.8	0.42	813.2	1604.02	1262.44	5.6	1.4	9	6.4	5.6	0.9	7.3	8	1.2	2.4
GB 12	8.8	7.4	2602.2	1.16	0.36	2.8	0.6	1019.46	1178.46	947.26	3.4	1.6	5.2	2.2	5.8	0.56	11.06	8.8	1.2	3.4
GB 13	8	8	2401.8	0.28	0.84	2.2	0.64	954	1404.32	397.66	3.8	1.3	5.8	7.6	8.4	1.18	13.34	7.8	1.6	3
GB 14	2.4	6.8	1590.4	0.44	1.2	2.8	0.84	1399.4	891.3	553.74	3.2	9	5.8	6.2	4.8	0.84	12.68	8.2	1	3.6
GB 15	3.2	6.6	1822.2	0.44	0.5	3.2	0.68	1333.8	1222.76	600	2.6	1	4.6	7.2	6	1.12	9.08	3.4	0.8	3
GB 16	3.2	7.2	2202.4	0.76	0.44	4.8	1.08	945.2	1032.24	619.84	3.8	1.06	4.2	7.8	6.8	1.38	9.76	3.6	1.4	1.8
GB 17	6.8	5	1822	0.9	0.46	3.2	0.66	1222.4	807.12	1244.4	3.2	1.62	4.6	5	2.6	0.92	8.78	3.6	0.8	3.8
GB 18	4.6	9	1202.2	1.1	1.44	6.4	0.66	647.8	1196.42	575.92	3.6	1.5	4.2	8.2	4.2	0.44	15.78	7.2	0.6	7.8
GB 19	7.6	8	1435.4	0.7	0.46	4.4	0.96	915.2	1197.4	575.6	2.4	1.58	6.4	3.2	6	0.52	7.94	9	0.8	6.8
GB 20	7.6	7.6	1644.4	1.76	0.6	3	0.76	1068.4	1381.82	850.22	2.4	1.38	2.6	3.6	6.6	1.12	17.58	9	0.6	5.4
Average	7.17	6.71	1869.29	0.768	0.69	5.07	0.62	1029.80	1097.39	633.16	3.41	1.64	6.01	5.56	5.58	0.89	10.40	6.82	1.14	4.56

ISSN 0795 - 22066

Table 2: The concentrations (wt %) of the major oxides in the shales from Gamba formation.

Sample	SiO_2 %	Al_2O_3 %	Fe_2O_3 %	TiO_2 %	MgO %	K_2O %	P_2O_5 %	SO_3 %	ZrO_2 %	SrO %	MnO %	Pr_6O_{11}%	CaO %	Cl %	LOI
GB 01	56.86	17.61	12.86	2.41	4.1	1.53	0.81	0.52	0.11	0.07	0.07	0	2.46	0.31	0.28
GB 02	54.4	17.38	16.39	2.51		1.41	0.63	0.27	0.15	0.35	0.3	0.07	2.45	0.13	3.56
GB 03	58.49	14.45	13.1	1.68	6.4	1.31	0.87	0.46	0.08	0	0.32	0	2.26	0.29	0.29
GB 04	58.56	13.75	13.18	1.85	6.4	1.36	0.93	0.48	0.1	0	0.38	0	2.45	0.3	0.26
GB 05	57.61	14.58	12.67	1.72	6.4	1.34	0.87	1.12	0.09	0	0.2	0.08	2.82	0.33	0.17
GB 06	53.18	12.98	18.91	1.46	6	0.99	0.89	0.45	0.06	0.09	2.03	0	2.33	0.24	0.39
GB 07	57.36	11.61	14.01	1.59	7.5	0.97	1.4	0.94	0.08	0	1.08	0	2.71	0.27	0.48
GB 08	54.64	14.45	15.24	1.79	5.3	1.37	0.93	0.43	0.08	0	0.46	0.05	4.6	0.24	0.42
GB 09	55.88	14.96	14.5	1.89	5.7	1.56	0.86	0.4	0.08	0	0.49	0.05	3.7	0.3	-0.37
GB 10	56.34	12.97	16.87	1.86	5.7	1.44	0.88	0.44	0.12	0	0.45	0	2.43	0.2	0.3
GB 11	49.01	12.91	15.97	1.63	5.2	1.15	0.69	0.38	0.06	0	0.36	0	12.06	0.24	0.34
GB 12	49.41	12.18	18.31	1.74	5.6	1.09	0.88	0.57	0.07	0.06	1.11	0	8.47	0.27	0.24
GB 13	51.14	13.82	18.86	1.69	0	1.14	0.68	0.41	0.07	0	0.1	0	11.46	0.26	0.37
GB 14	57.64	16.25	13.53	2.03	4.9	1.33	0.72	0.49	0.11	0.09	0.06	0	2.37	0.32	0.16
GB 15	57.56	14.39	12.69	1.76	6.7	1.39	1.06	0.51	0.07	0	0.21	0	3.12	0.29	0.25
GB 16	55.03	17.22	15.3	2.45	3.8	1.44	0.78	0.52	0.11	0.13	0.1	0.05	2.56	0.27	0.24
GB 17	55.99	16.43	14.72	2.08	4.8	1.4	0.74	0.54	0.1	0	0.1	0	2.29	0.57	0.24
GB 18	56.58	11.31	12.12	2.85	3.2	1.14	3.78	0.51	0.26	0	0.37	0	7.31	0.24	0.33
GB 19	54.51	16.63	16.96	2.27	3.7	0	0.66	0.54	0.1	0.1	0.15	0.07	2.39	0.28	1.64
GB 20	58.76	13.56	15.53	1.76	6.2	1.35	0.89	0.38	0	0.09	0.51	0.06	2.3	0.29	-1.68

ISSN 0795 - 22066

STATISTICAL ANALYSIS

A multivariate statistical method was used to examine the bulk chemical data using IBM SPSS-19.0 statistical software, with a focus on the trace elements (ppm) found in the shales derived from the Sokoto Basin. A factor analysis with varimax rotation was performed on the correlation matrix of reorganized data from three distinct groups of elements. The square loadings of the variables were calculated based on the eigenvalues' variance, cumulative sums, and extraction sums. To achieve a new set of factors with minimal overlap, the axis determined by factor analysis was rotated to group the original variables. Following this, the current dataset underwent factor analysis to delineate the impact of variables with lower significance (factor score of 0.4). This method allows the varimax rotation of various varifactors with eigenvalues greater than 1 to be further refined. As a result, the original variables are more prominently displayed in the varifactors. [46] classified the factor loading into categories of "strong," "moderate," and "weak," based on the absolute loading values exceeding 0.75, ranging from 0.75 to 0.50, and falling between 0.50 and 0.40, respectively. To evaluate the level of dissolution in the major component matrix and to recognize the chemical processes, factor and cluster analyses were employed. Following normalization to zero mean and unit variance as suggested by Massart *et al.* [47], the data underwent hierarchical agglomerative clustering utilizing squared Euclidean distances as the similarity metric. The Wards technique was chosen based on its efficacy in grouping mechanisms, as it incorporates a greater amount of information regarding cluster contents compared to alternative methods [48, 49]. Furthermore, it exhibits a minimal impact on space distortion.

RESULTS AND DISCUSSION

ELEMENTS DISTRIBUTION

The concentrations of the elements within the shales taken from the Gamba Formation are shown in Table 1. The average concentrations of the elements (Barium (Ba), Bismuth (Bi), Calcium (Ca), Cerium (Ce), Europium (Eu), Gadolinium (Gd), Hafnium (Hf), Potassium (K), Magnesium (Mg), Sodium (Na), Terbium (Tb), Niobium (Nb), Praseodymium (Pr), Samarium (Sm), Strontium (Sr), Tantalum (Ta), Thorium (Th), Titalium (Ti), Uranium (U), and Zinc (Zn)) ranged from 1.14 to 1869.29 ppm, respectively (Table 1). Alkali metal and alkaline earth metal constituents, namely Na, K, Ca, and Mg, were present in significantly elevated levels within the shale samples, with U exhibiting the lowest values (Fig. 3, Table 1). These alkali metal and alkali-earth metal elements are more susceptible to weathering, therefore, their high concentrations in these shales show that the Gamba shales have

ISSN 0795 - 22066

experienced little or no weathering. Also, the detritus derived from various provenances (such as feldspars and dolomites) may be responsible for these high concentrations.

The levels of rare earth elements (REEs) within the Gamba Formation exhibit a variation from 12.94 to 30.48 ppm, with an average of 19.73 ppm as shown in Table 3. The proportions of light rare earth elements (LREEs) to heavy rare earth elements (HREEs) present in the shales of the Gamba Formation range from 0.93 to 3.77, with an average of 1.84, as depicted in Table 3.

Compared with HREEs, LREEs are more enriched in the shale samples (Table 3), which is consistent with the general distribution of REEs in shale [50]. This pattern of LREE enrichment and HREE depletion is commonly observed in sedimentary rocks, where the LREEs are preferentially incorporated into the mineral lattice of detrital minerals and organic matter during weathering and transport processes [51].

Table 3: Geochemical parameters computed from the rare earth elements (REEs) in the shales.

Sample (ppm)	∑RREs	ΣLREEs	ΣHREEs	LREEs/HREEs
GB 01	19.6	13.2	9.6	1.38
GB 02	21.54	14.34	9.6	1.49
GB 03	23.58	16.18	10.4	1.56
GB 04	30.48	19.28	15	1.29
GB 05	25.06	15.46	13.2	1.17
GB 06	19.98	15.38	9.8	1.57
GB 07	15.9	12.5	6.6	1.89
GB 08	19.74	15.34	7.6	2.02
GB 09	16.32	9.72	10.4	0.93
GB 10	20.66	15.66	7.8	2.01
GB 11	20.74	17.94	8.4	2.14
GB 12	13.32	10.52	6.2	1.70
GB 13	18.02	15.82	6	2.64
GB 14	25.44	22.64	6	3.77
GB 15	16.94	13.74	5.8	2.37
GB 16	19.06	14.26	8.6	1.66
GB 17	15.78	12.58	6.4	1.97
GB 18	22.84	16.44	10	1.64
GB 19	16.74	12.34	6.8	1.81
GB 20	12.94	9.94	5.4	1.84
Average	19.73	14.66	8.48	1.84

ISSN 0795 - 22066

The distribution of REEs provides insight into the depositional environment and source of organic matter. For example, the REEs pattern distinguishes between marine and lacustrine depositional environments [52]. Sediments deposited in oxygen-depleted deeper aquatic environments tend to contain higher concentrations of LREE (Light Rare Earth Element), whereas HREE (Heavy Rare Earth Element) is more abundant in oxygen-rich surface waters [53]. Additionally, Rare Earth Elements (REEs) like Cerium (Ce) have been utilized as indicators of redox conditions. Cerium exists in two oxidation states, Ce^{3+} and Ce^{4+}, which are determined by the prevailing redox environment. The fractionation of Cerium in comparison to its neighboring elements is a direct consequence of the fluctuating oxidation states [54]. The trace elements data are normalized by the UCC (average upper continental crust, Taylor and McLennan, [55] and PAAS (average upper continental crust, Taylor and McLennan, [55]; Fig. 4). The elements show similar distribution patterns on the UCC and PAAS. Bi is found enriched on these plots while Zn, Nb, Hf, Ta, Sr, Ba, Th, and U are depleted (Fig. 4).

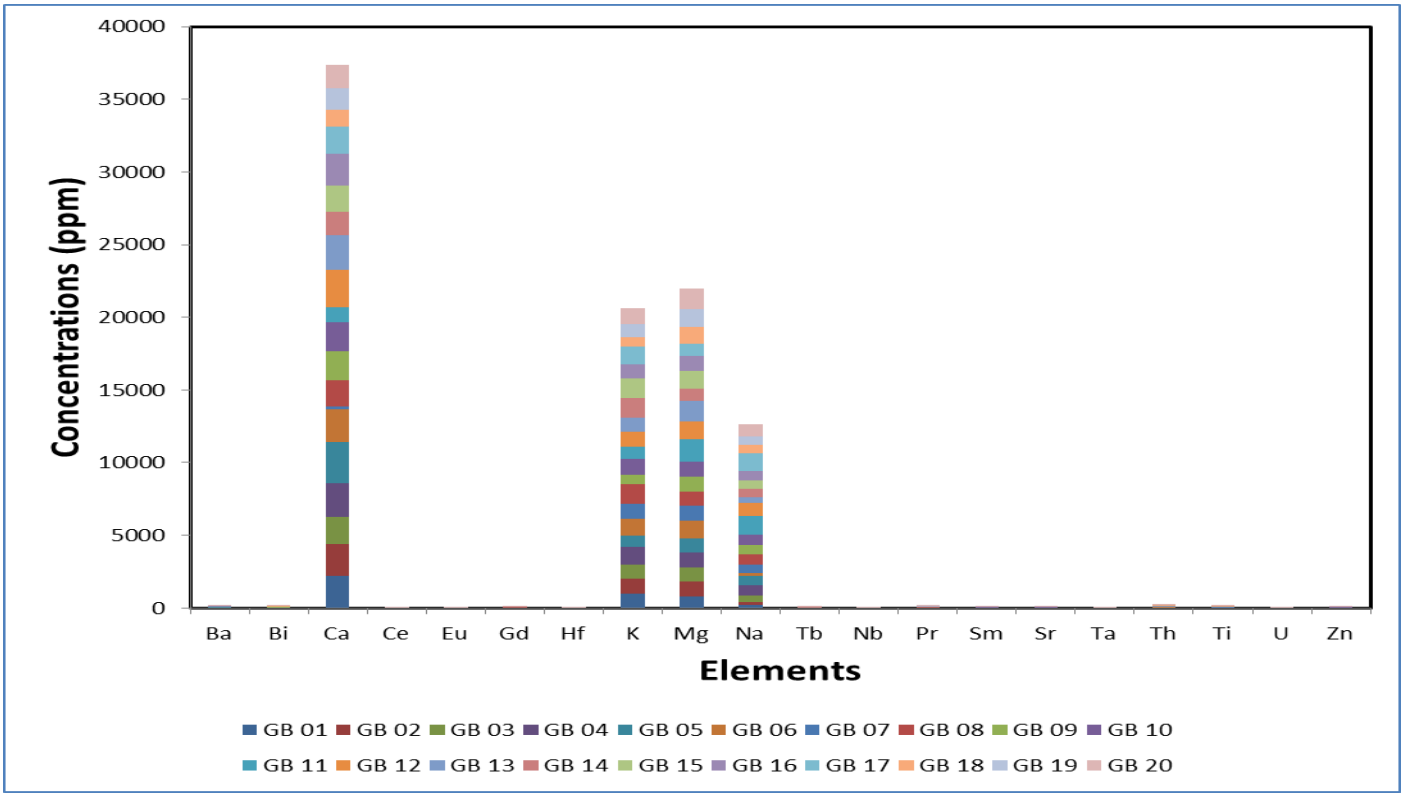

Fig. 3: The histogram of the concentrations of the elements showing their distributions in the studied shales.

ISSN 0795 - 22066

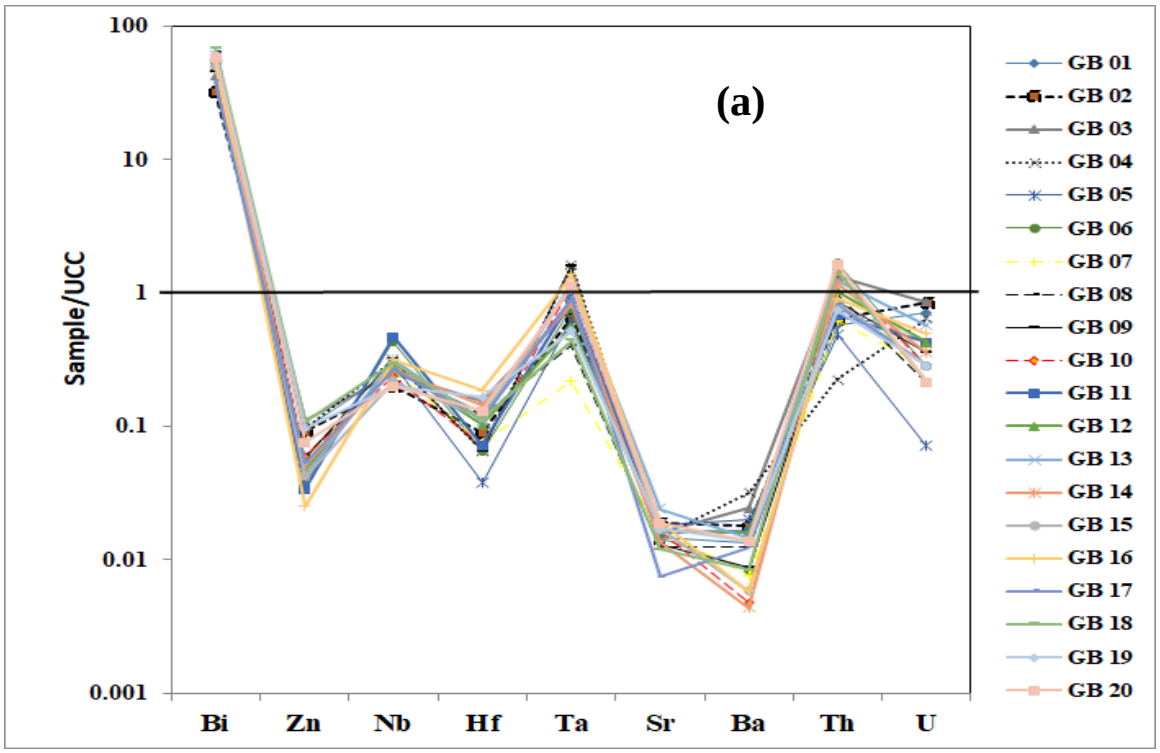

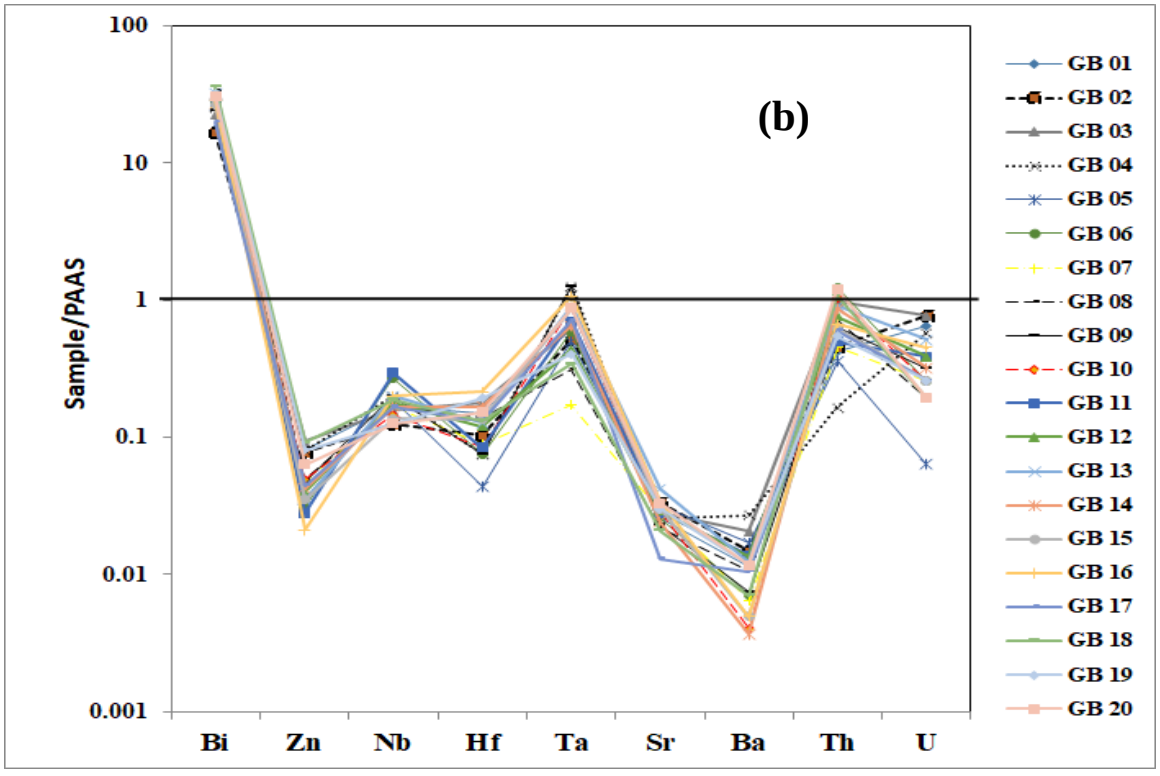

Fig. 4: The spider diagrams of the (a) PAAS and (b) UCC normalized trace elements showing their ditributions in the shales.

ISSN 0795 - 22066

MAJOR OXIDES DISTRIBUTION

The concentrations of the major oxide constituents in the shales collected from the Gamba Formation are shown in Table 2. A total of fourteen (14) major oxides were detected in the shales and this includes SiO_2, Al_2O_3, Fe_2O_3, TiO_2, MgO, K_2O, P_2O_5, SO_3, ZrO_2, SrO, MnO, Pr_6O_{11}, CaO, and Cl (Table 2). The average concentrations of the major oxides range from 0.02 to 55.45 % (Table 2, Fig. 5). SiO_2 has the highest concentration with an average value of 55.45 %. SiO_2 is derived from the remains of ancient marine organisms that lived in the ocean where the shales were deposited [56]. This is followed by Fe_2O_3 and Al_2O_3 with average values of 15.09 % and 14.47 %, respectively (Table 2, Fig. 5) while the concentrations of the other oxides are generally low (Table 2, Fig. 5). According to Yang and Du [57], Al_2O_3 and Fe_2O_3 are derived from the weathering of aluminum- and iron-rich minerals that were present in the shales source area. Also, the presence of calcium oxide (CaO; an average of 4.13%) and magnesium oxide (MgO; an average of 5.04%) in the shales in relatively high quantities suggest marine input and weathering of calcium- and magnesium-rich minerals in the source rock [56] . This pattern of distribution has been previously reported in Eocene to Recent sediments from the Western Niger Delta, Nigeria [58]. Furthermore, Pundaree *et al*.[59] noted that mafic rocks predominantly consist of Fe_2O_3 and MgO. Therefore, the elevated levels of Fe_2O_3 (with an average of 15.09%) and MgO (with an average of 5.04%) in the samples indicate that the source rocks are likely to be mafic to ultramafic. Sodium oxide (Na_2O) could not be detected from the Gamba shales, the absence of Na_2O in shale samples can indicate that the shale was deposited in a reducing environment. Under reducing conditions, sodium ions can be removed from the sediment through reactions with organic matter or sulfides. Additionally, if the depositional basin was located far from the source of sodium-rich minerals, there may not be enough sodium available to form Na_2O. The high percentage of SiO_2 in Gamba shale samples which ranged from 41.09 % to 58.8 % having an average of 55.45 % (Table 2) suggests that the rock is likely a quartz-rich sedimentary rock, such as sandstone, which is resistant to weathering due to its high quartz content [1]. However, the presence of Fe_2O_3 ranges from 12.12 % to 18.97 % with an average of 15.09 % and that of Al_2O_3 which ranges from 11.31 % to 17.61 % with an average of 14.47 % (Table 2) is both significant amounts indicates that the rock has undergone some degree of weathering, as these oxides are typically associated with the breakdown of iron-rich minerals and feldspars, respectively [60]. The titanium dioxide (TiO_2) concentrations within the shale samples exhibit a range of values from 1.46% to 2.85%, with a mean value of 1.95%

ISSN 0795 - 22066

as indicated in Table 2. This average value is notably lower when compared with the corresponding values for the Post Archean Australian Shale (PAAS) and Upper Continental Crust (UCC) as illustrated in Figure 6.

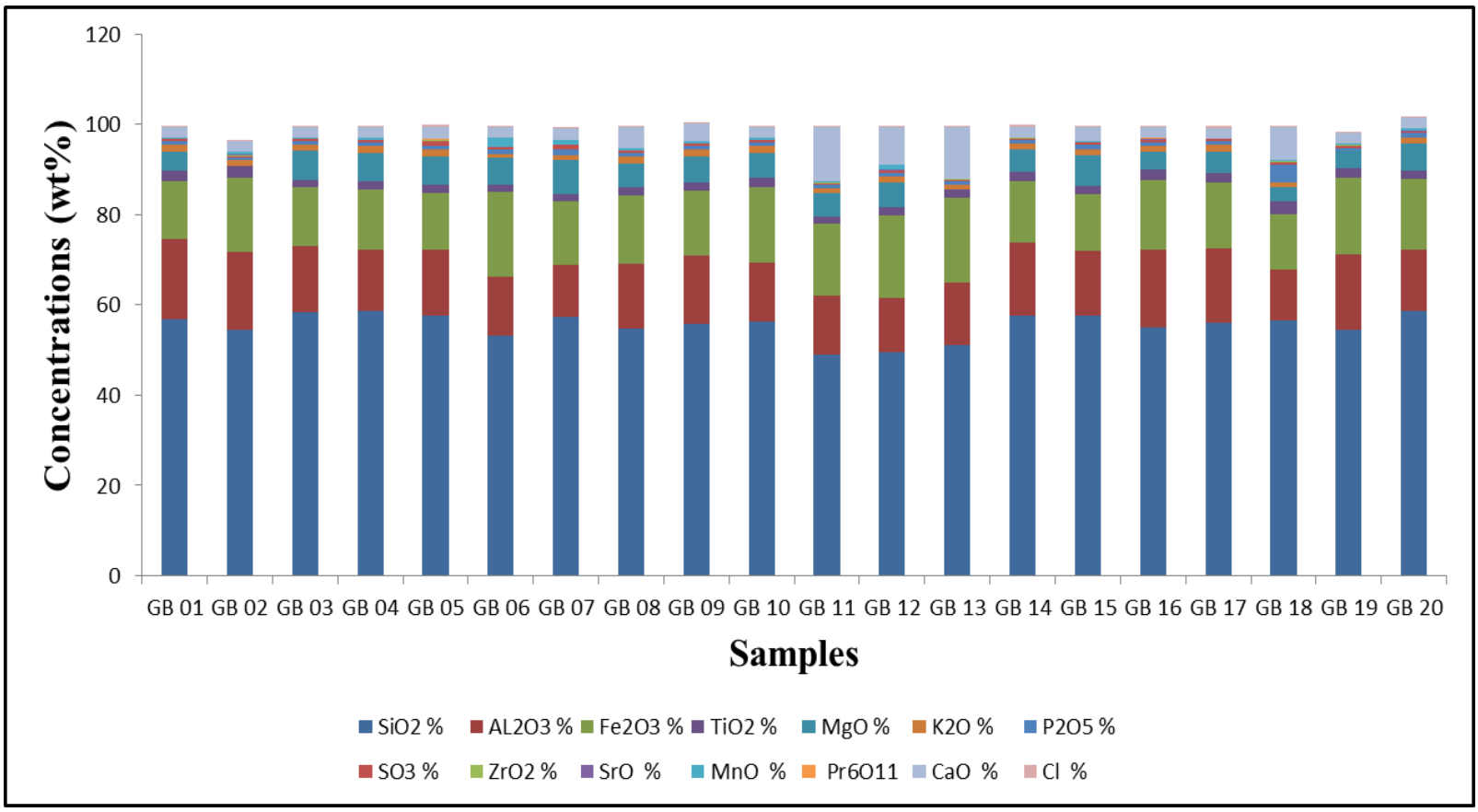

Fig. 5: The histogram of the contents of the major oxides in the studied shales showing their variations in the studied shales.

This further suggests that the source rock for these shales was mafic to ultramafic rock [59]. The concentrations of most of the oxides are depleted to PAAS and UCC (Table 2, Fig. 6). However, the contents of SiO_2, and Al_2O_3 are enriched compared with those of PAAS and UCC (Table 2, Fig. 6). The trace element oxide distributions as plotted in Figures 7 and 8 generally show no obvious correlations, which probably imply that these major oxides are not only hosted by clay minerals [10]. Except for K_2O, SiO_2, and TiO_2, the other oxides weakly follow the trend of negative correlation (increasing as Al_2O_3 increases), indicating that quartz content is not influenced by a special paleoenvironment favoring the growth of siliceous tests and skeletons (e.g. radiolarian or siliceous

ISSN 0795 - 22066

sponges) [11]. Also, Fe_2O_3, MnO, and CaO show negative correlations on the plots of SiO_2 versus major elements (figures 9 and 10) while others are positive which further suggests that they are associated with micaceous and/or clay minerals in the sediments [59]. A negative relationship between CaO and MgO is detected, suggesting that these shales are composed of minerals other than carbonates (Fig. 10d). Considering the lower LOI which is mainly attributed to losses of CO_2 and organic matters (Table 2), enrichment of CaO and MgO in these shales is possibly resulted from carbonate minerals.

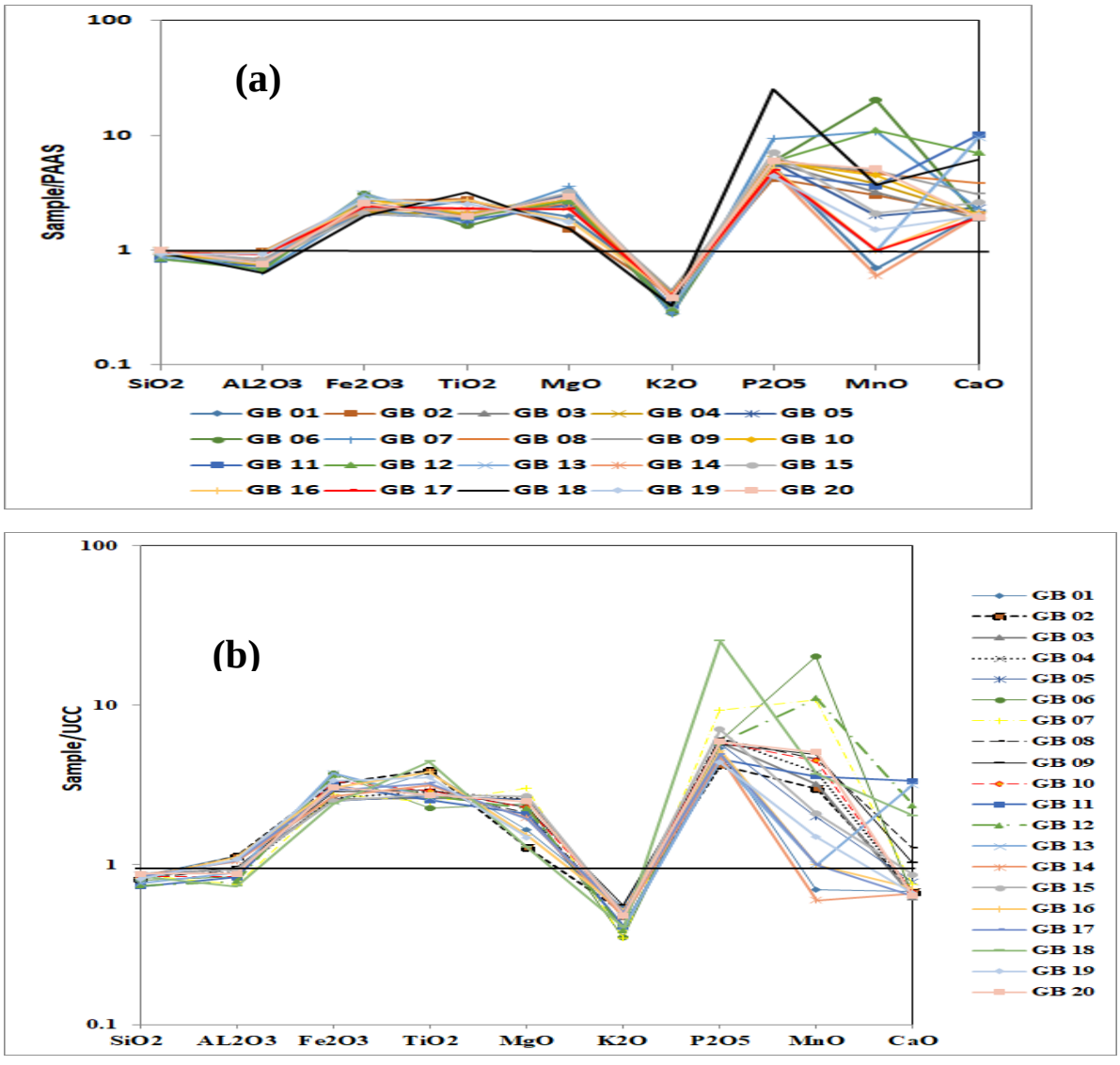

Fig. 6: The spider diagrams of the (a) PAAS and (b) UCC normalized major oxides showing their distributions in the Gamba shales

ISSN 0795 - 22066

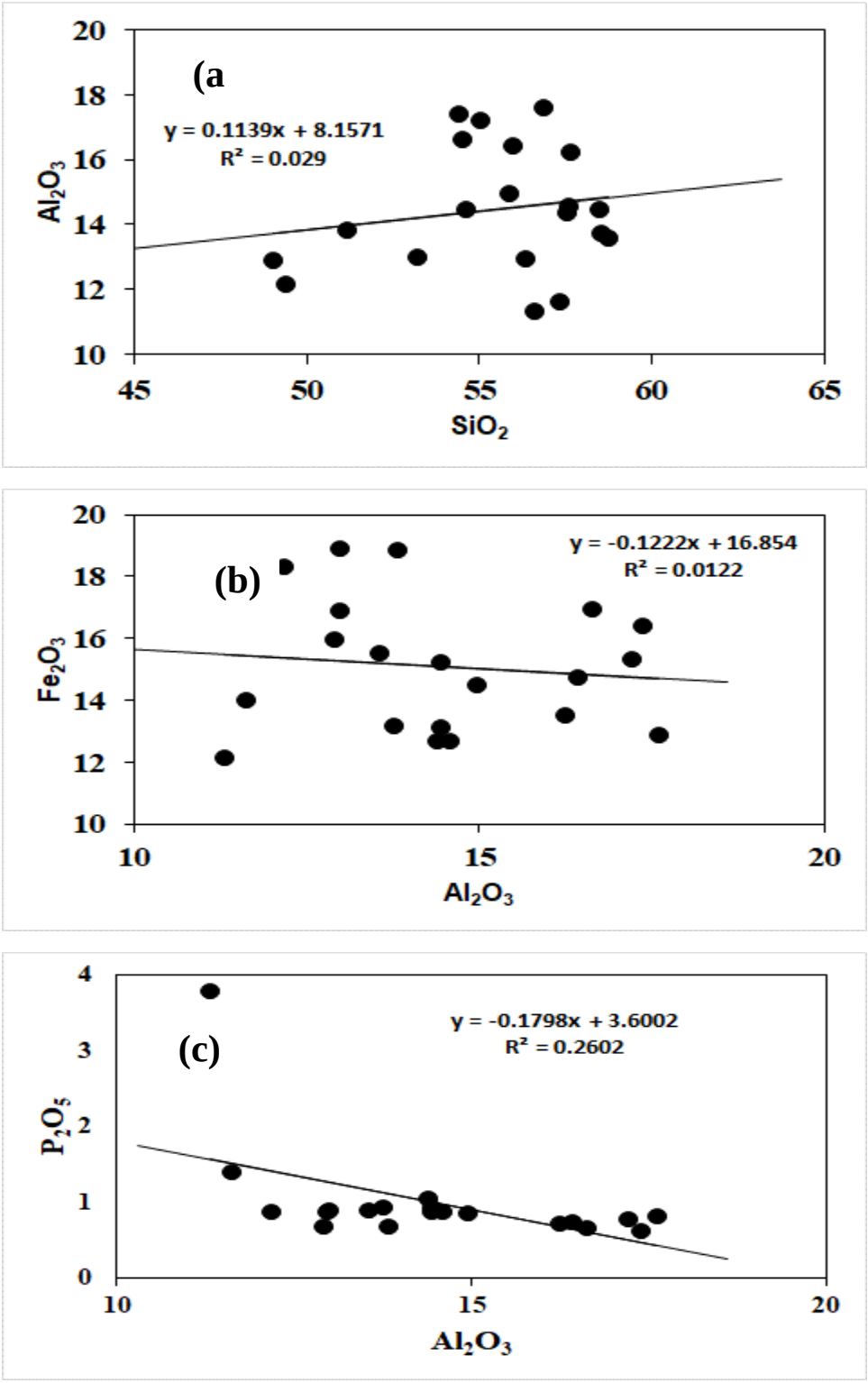

Fig. 7: Correlation plots of Al_2O_3 vs (a) SiO_2, (b) Fe_2O_3, and (c) P_2O_5 in Gamba shales showing the relationship among Al_2O_3 and other oxides

ISSN 0795 - 22066

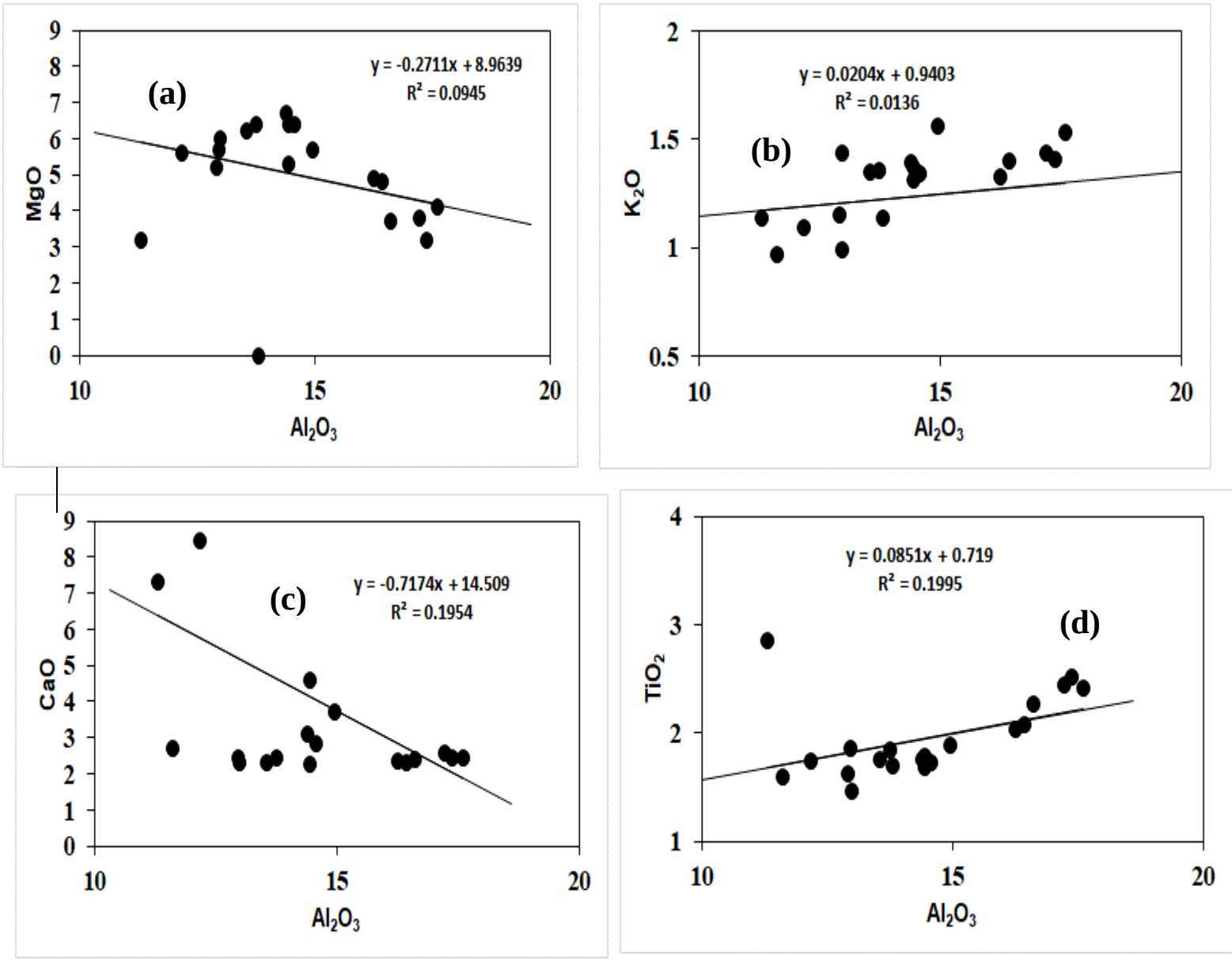

Fig. 8: Correlation plots of Al_2O_3 vs (a) MgO, (b) K_2O, (c) CaO, and (d) TiO_2 in Gamba shales showing the relationship among Al_2O_3 and other oxides

ISSN 0795 - 22066

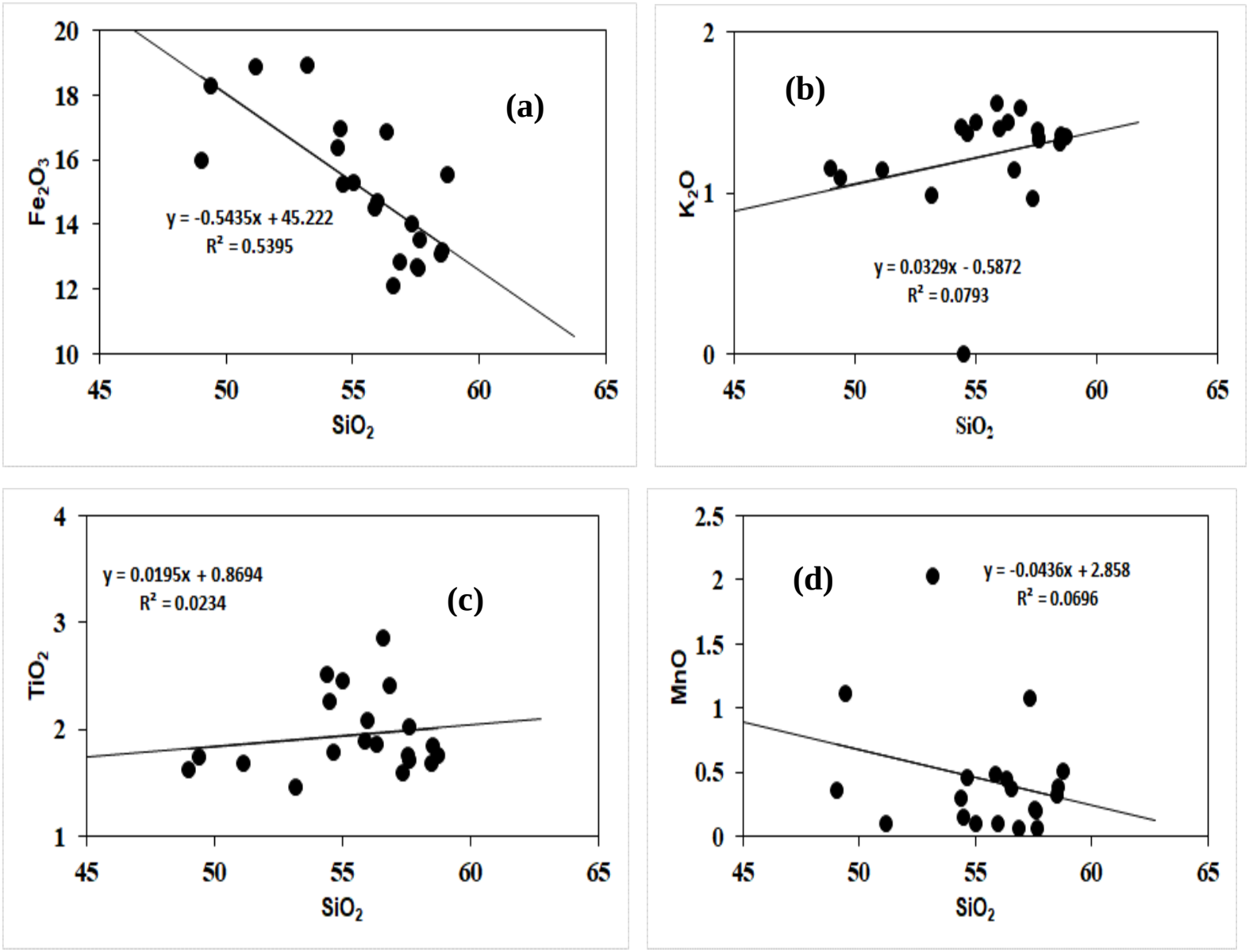

Fig. 9: Correlation plots of SiO_2 vs (a) Fe_2O_3, (b) K_2O, (c) TiO_2, and (d) MnO in Gamba shales showing the relationship among SiO_2 and other oxides.

ISSN 0795 - 22066

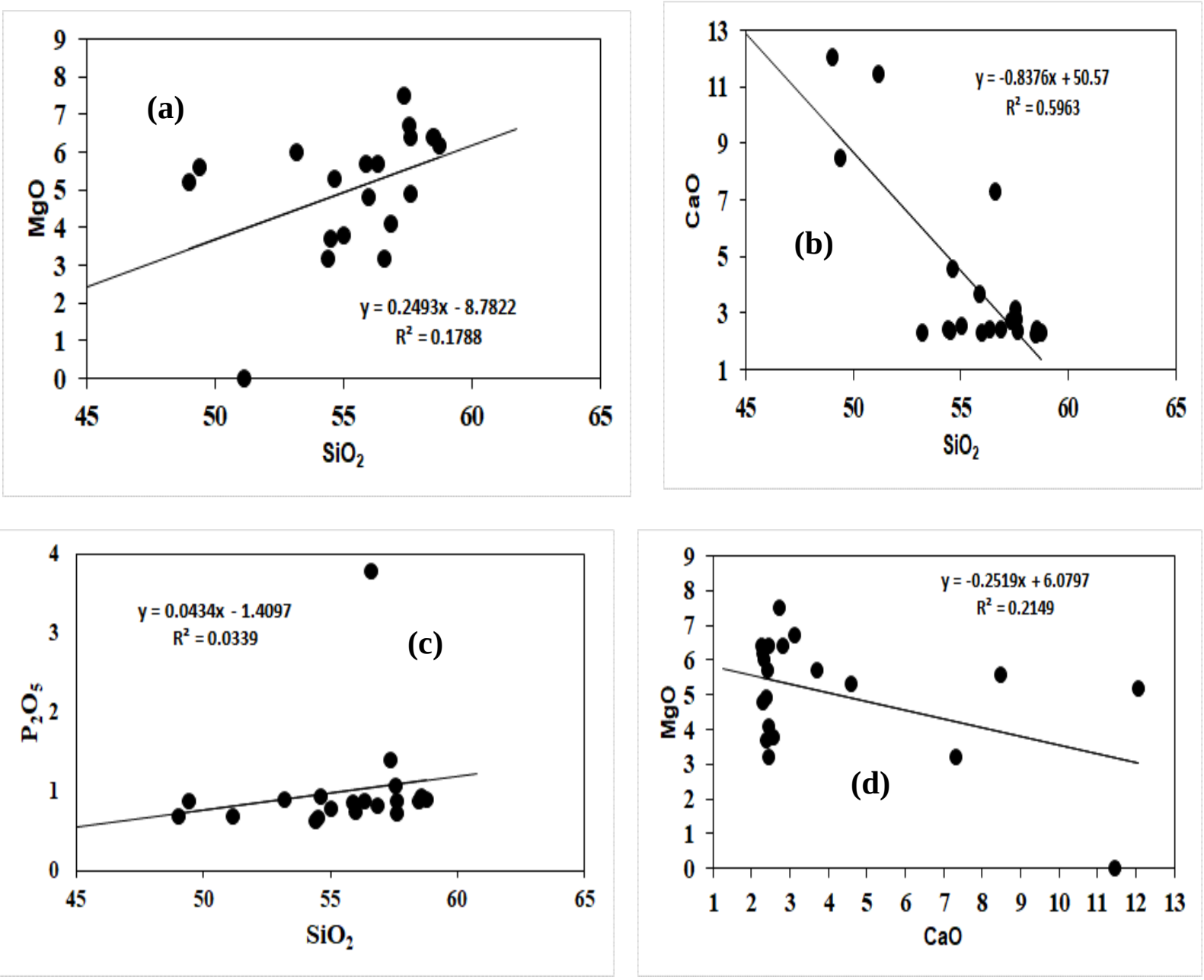

Fig. 10: Correlation plots of SiO_2 vs (a) MgO, (b) CaO, (c) $P2O_5$, and (d) Plot of MgO vs. CaO in Gamba shales showing the relationship among SiO_2 and other oxides.

PALEO-REDOX CONDITIONS

The understanding of the depositional setting of the geological materials is enhanced by the geochemical parameters of trace elements. Redox conditions influence the distribution of trace elements like uranium (U) and thorium (Th), with their relative abundances serving as indicators of oxygenated (oxic) versus oxygen-depleted (anoxic) environments, as discussed by Akinyemi *et al*.

ISSN 0795 - 22066

[61] and Liu *et al*. [19]. Thorium exhibits a certain degree of stability in the presence of oxygen, whereas the presence of reducing conditions and organic matter (either in sediment or immediately beneath the sediment-water interface) enhances the fixation of aqueous Uranium [62]. Consequently, the ratios of Uranium to Thorium serve as indicators of the prevailing redox conditions [63]. Nevertheless, the concentrations of Uranium and Thorium may also be affected by volcanic eruptions and hydrothermal processes during the period of deposition and early diagenesis [64]. Jones and Manning [63] proposed that U/Th values less than 0.75 are indicative of oxic depositional conditions, whereas values ranging from 0.75 to 1.25 suggest dysoxic conditions. Values exceeding 1.25, on the other hand, are associated with suboxic to anoxic depositional conditions. The present investigation examined the U/Th values which varied between 0.03 and 0.74 (Table 4), suggesting the deposition of shales occurred in an oxygenated environment. Similarly, Wignall and Twitchett [65] have previously reported that Th/U values that vary between 2 and 7, and > 7 suggest oxic depositional conditions while values < 2 depict suboxic to anoxic conditions. The current investigation observed a range of Th/U values between 1.34 and 26.30 (Table 4), indicating the prevalence of oxic depositional environments in the shale Formations. Similarly, the assessment of authigenic uranium (authigenic U =Total U-(Th/3)) serves as a valuable indicator for determining the paleo-redox conditions in marine settings, as proposed by Wignall and Myers [66]. The values of U-(Th/3) < 2 suggest oxic conditions while values > 2 indicate suboxic to anoxic conditions [66]. In our study, the values of U-(Th/3) ranged from -0.07 to 0.99 (Table 4), supporting oxic depositional conditions for the shales.

PALEOSALINITY AND DETRITAL INFLUX

Sr and Ba serve as indicators of ancient salinity levels according to previous studies [67, 68, 69]. The utilization of Sr/Ba ratios is common for investigating past salinity conditions in sedimentary settings [22, 23]. High Sr/Ba ratios are typically indicative of elevated salinity levels, while lower ratios are associated with decreased salinity according to Deng and Qian [68]. The Sr/Ba ratio is below 1.0 in sediment samples from freshwater bodies, exceeding 1.0 in marine sediment, and falling within the range of 0.5 to 1.0 in brackish water environments as reported by Wei *et al*. [70]. The relationship between Sr/Ba ratios and salinity is positively correlated in contemporary as well as historical lacustrine settings as indicated by Wei and Algeo [71]. Within the scope of this investigation, the Sr/Ba values observed in the shales spanned from 0.38 to 2.23 (refer to

ISSN 0795 - 22066

Table 4), demonstrating an average value of 1.02.

Table 4: Geochemical ratios computed from the elements and oxides in the shales.

Sample	U/Th	Sr/Ba	Eu/Eu*	Th/U	U-(Th/3)	Al_2O_3/TiO_2
GB 01	0.32	0.70	0.32	3.10	-0.07	7.31
GB 02	0.35	0.67	0.47	2.83	0.13	6.92
GB 03	0.17	0.42	0.23	5.93	-2.34	8.60
GB 04	0.74	0.30	0.45	1.34	0.99	7.43
GB 05	0.04	0.58	0.18	26.20	-1.55	8.48
GB 06	0.04	1.13	0.34	22.50	-5.20	8.89
GB 07	0.12	1.38	0.65	8.35	-1.43	7.30
GB 08	0.06	0.65	0.55	17.37	-2.87	8.07
GB 09	0.11	0.96	0.38	9.30	-2.10	7.92
GB 10	0.05	2.23	0.29	19.15	-4.31	6.97
GB 11	0.16	0.62	0.33	6.08	-1.23	7.92
GB 12	0.11	0.66	0.44	9.22	-2.49	7.00
GB 13	0.12	1.05	0.63	8.34	-2.85	8.18
GB 14	0.08	2.00	0.88	12.68	-3.23	8.00
GB 15	0.09	1.88	0.32	11.35	-2.23	8.18
GB 16	0.14	2.13	0.22	6.97	-1.85	7.03
GB 17	0.09	0.38	0.35	10.98	-2.13	7.90
GB 18	0.04	0.91	0.61	26.30	-4.66	3.97
GB 19	0.10	0.79	0.37	9.93	-1.85	7.33
GB 20	0.03	0.87	0.56	29.30	-5.26	7.70
Average	0.15	1.02	0.43	12.36	-2.33	7.56

This suggests the coexistence of a marine sedimentary milieu alongside a transitional sedimentary environment. A lack of association between Sr/Ba and U/Th is apparent (Fig. 11a). Elevated Sr/Ba ratios are concurrent with diminished U/Th ratios, potentially indicating the presence of certain shales that were deposited in relatively shallow environments characterized by increased oxygen levels. The decreased Sr/Ba ratios, likely resulting from a combination of heightened terrigenous input, elevated water levels, and reduced water salinity, may suggest a decline in oxygen levels in deeper water, as supported by the corresponding increase in U/Th ratios [10]. In addition, Sr/Ba shows a negative correlation with CaO (Fig. 11b), suggesting that the Sr/Ba ratios are not influenced by carbonate minerals in the shale samples. The cross plots of Sr against Ba show a weak positive correlation (Fig. 11c), implying that Sr and

ISSN 0795 - 22066

Ba are weakly constrained by similar factors in this study. Typically, elevated levels of P_2O_5 are commonly found in dysaerobic water close to the transition between oxic and anoxic conditions; therefore, fluvial swamps exhibit relatively low (0.01%) P_2O_5 [72]. The P_2O_5 concentrations range from 0.63 wt% to 3.78 wt% in the analyzed shales, indicating the influence of fluvial processes (Table 2). The increased P_2O_5 levels identified in GB-07 and GB-18 could be attributed to the influx of detrital material with high mineral contents [61].

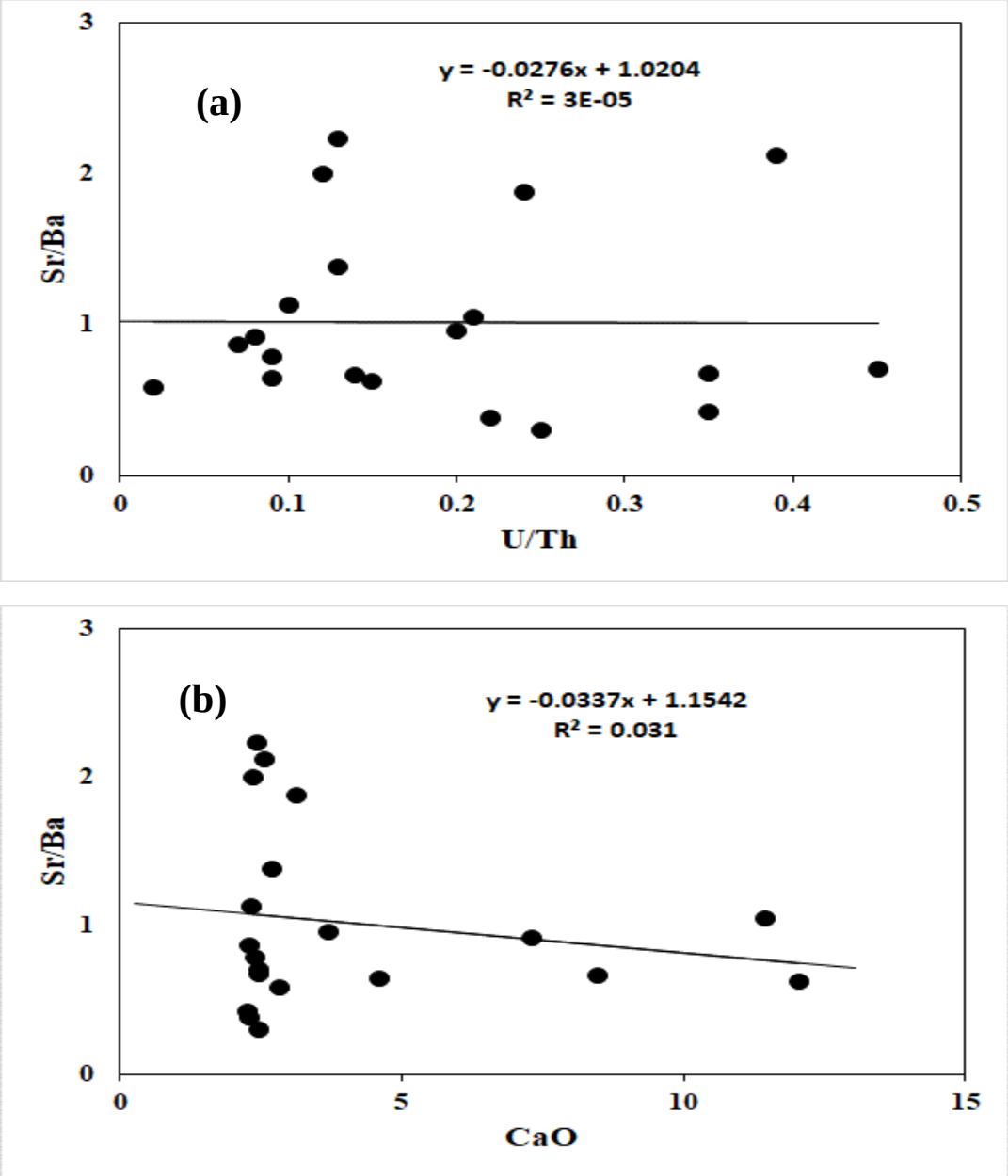

ISSN 0795 - 22066

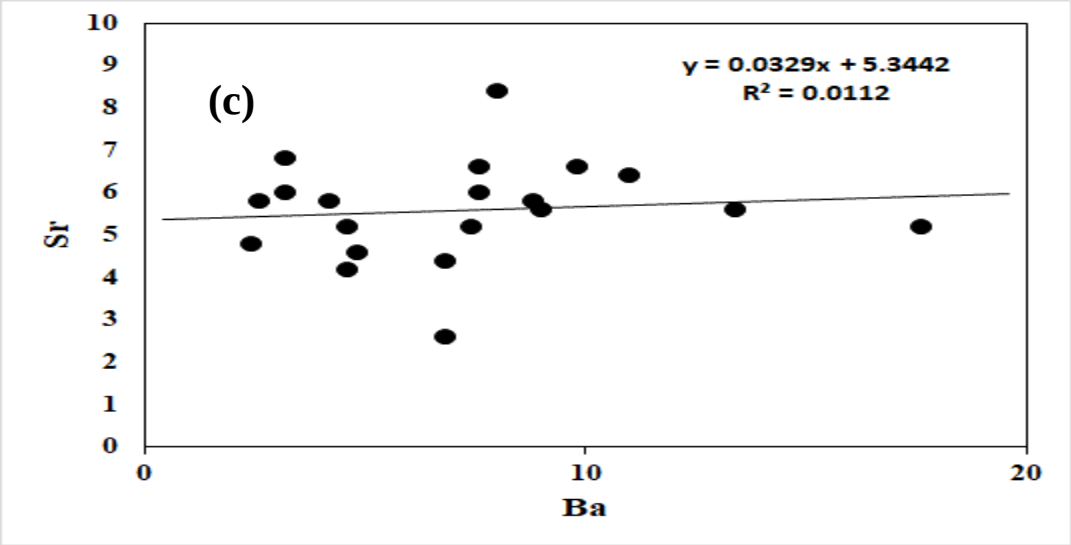

Fig. 11: Cross plots of Sr/Ba vs (a) U/Th, (b) CaO, and (d) Plot of Sr vs. Ba in Gamba Shales.

PROVENANCE

The discrimination diagram suggested by Roser and Korsch [2] for categorizing the origins of sediments into four provenance zones - mafic, intermediate, felsic, and igneous provenances - was not applicable in the current study as Na_2O was lacking among the major oxides. Nevertheless, the ratios of Th/U, Eu/Eu*, and Al_2O_3/TiO_2 were employed. Elevated concentrations of thorium compared to uranium may suggest a source with felsic characteristics. The ratio of thorium to uranium, frequently employed in the context of thorium and uranium concentrations within weathering processes under oxidizing environments, has been utilized for establishing the felsic origin [73, 74]. Weathering in the presence of oxidizing conditions leads to the dispersion of uranium in the form of U^{6+}, while thorium (Th) remains stationary. Consequently, there is a notable rise in the Th/U ratio. Elevated levels of incompatible elements such as Th suggest an origin from felsic rather than mafic sources. Examples of such materials include granodiorite derived from ancient upper continental crust and felsic gneisses. The utilization of the Th/U ratio is restricted to sedimentary rocks exclusively. Within this investigation, the mean Th/U value is recorded as 12.36 (Table 4), indicating the presence of felsic source rocks. Analysis of the Th vs. Th/U graph [74,75] reveals that, throughout the process of weathering, there is a marked increase in the Th/U ratio (surpassing the standard upper crustal igneous values of 3.5-4.0), particularly noticeable in the majority of samples derived from the Gamba Formation, with three samples displaying values below this

ISSN 0795 - 22066

threshold (Fig. 12). Such relatively low Th/U ratios are frequently documented in sediments found along active margins [74]. Furthermore, the utilization of the europium anomaly (Eu/Eu*) is frequently employed in the examination of the origin of sedimentary Formations. Broadly speaking, the atypical behavior of Eu signifies a past occurrence in a deoxidizing igneous setting that later transformed into the upper continental crust [55]. Rudnick [76] posited that the presence of a positive Eu anomaly can be primarily attributed to the influence of regions that are marked by hydrothermal vents or have a feldspar origin. Additionally, Oni *et al.* [77] documented that the solutions that emerged in environments where plagioclase acts as a stable residual component or in which plagioclase undergoes crystallization and subsequent loss are likely to exhibit a notable depletion in Eu, consequently displaying a negative Eu anomaly. Values exceeding 0.85 are indicative of a positive Eu anomaly, whereas values falling below 0.85 suggest a negative Eu anomaly; a value of exactly 0.85 signifies the absence of an anomaly [76, 77]. Within the scope of the current investigation, the range of Eu/Eu* values spans from 0.18 to 0.88, with a mean value of 0.43 (Table 4), denoting a negative Eu anomaly. Negative anomalies in felsic rocks and sediments are commonly attributed to processes such as lithospheric or intracrustal feldspar fractionation, as well as the alteration of feldspars during weathering phenomena [78]. Felsic igneous rocks typically exhibit elevated LREE/HREE ratios and more prominent negative Eu anomalies as presented in Table 3. Conversely, mafic igneous rocks are characterized by lower LREE/HREE ratios and a scarcity of Eu anomalies, according to Cullers [79]. Moreover, Cullers [5] postulated that Eu/Eu* values ranging from 0.48 to 0.78 predominantly originate from felsic rather than mafic sources, suggesting that the analyzed shales are predominantly of felsic sources.

Na, K, Ca, and Mg are typically depleted through the process of weathering in comparison to immobile elements such as Al, Ti, and Zr. Consequently, these immobile elements tend to be preserved within rocks throughout weathering procedures as indicated by various studies [8, 20, 80, 81]. Hence, the utilization of Al and Ti ratios in sediment samples is a prevalent method for identifying the origins of the rocks from which they were derived [8]. Previous research has documented Al_2O_3/TiO_2 weight ratios ranging from 3 to 8 for mafic igneous rocks, 8 to 21 for intermediate igneous rocks, and 21 to 70 for felsic igneous rocks [4]. The Al_2O_3/TiO_2 ratios observed in the Gamba shales exhibit a range from 3.97 to 8.89, with a mean value of 7.70 as presented in Table 4. These findings suggest that the precursor materials of the shales are indicative of

ISSN 0795 - 22066

intermediate igneous rock compositions. The cross plots of TiO_2 and K_2O against Al_2O_3 in Figure 13 show that shales are composed of basalt granite and muscovite minerals.

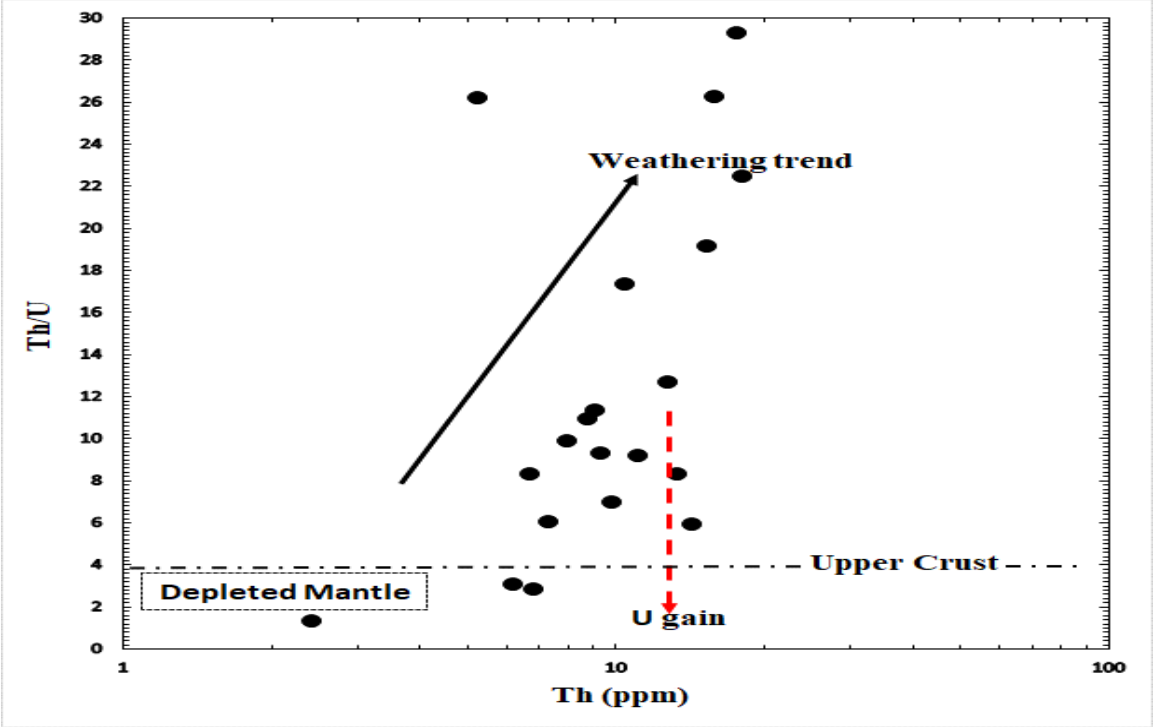

Fig. 12 : Th/U vs. Th plot for the formation. Fields and trends from [75].

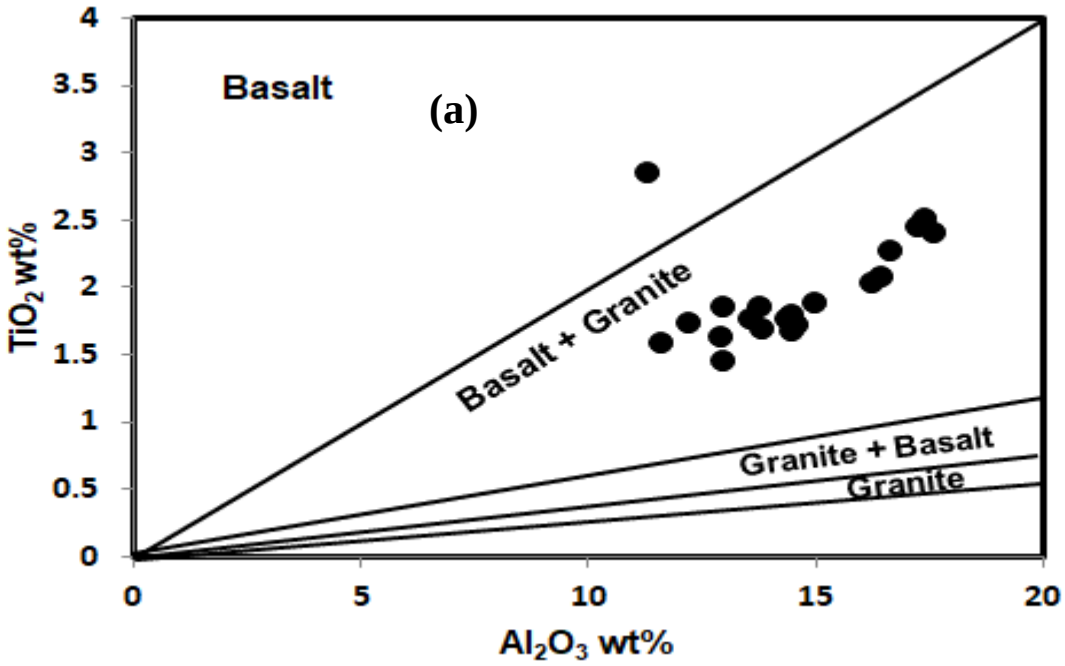

ISSN 0795 - 22066

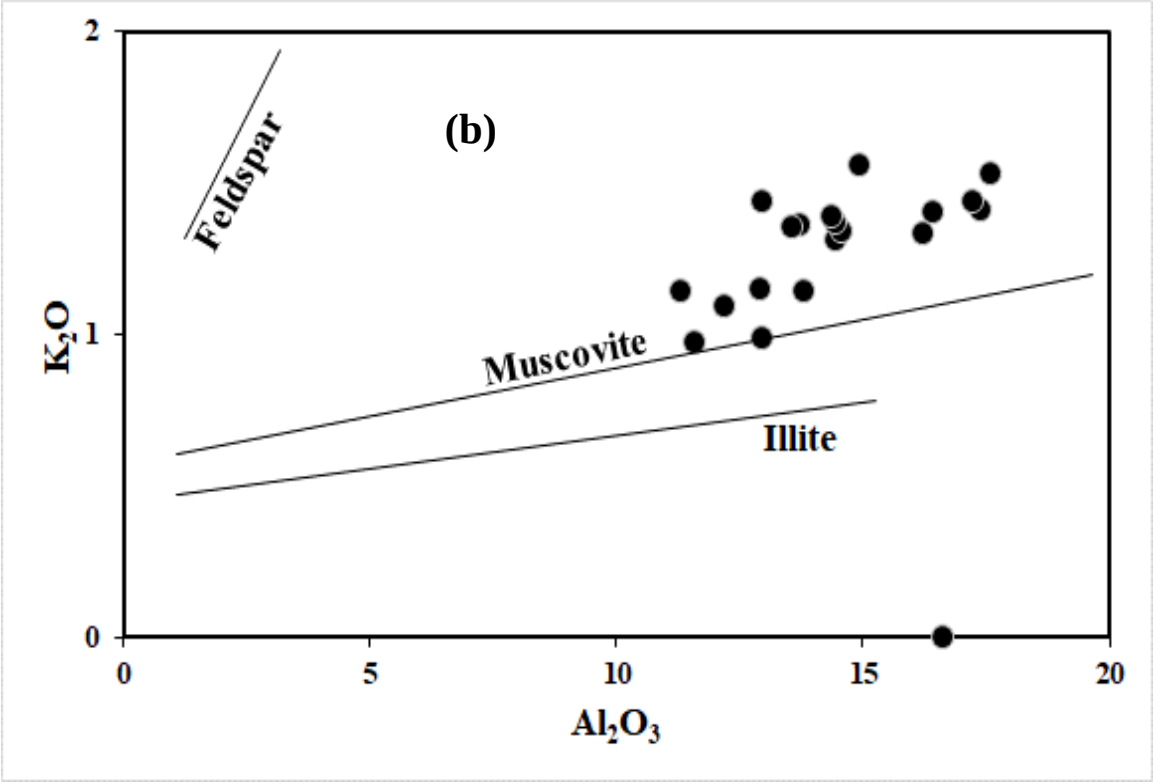

Fig. 13: Cross plots of Al_2O_3 vs (a) TiO_2 (after [4]) and (b) K_2O (after [4]) and (d) Plot of Sr vs. Ba in studied Shales showing the provenance of the Gamba formation

TECTONIC SETTINGS

Understanding the tectonic setting of a basin holds significance in the investigation of petroleum and other valuable commodities, as well as in the realm of paleogeography. Several researchers have highlighted the significance of employing major element geochemical analysis of sedimentary formations to deduce tectonic environments through the utilization of discrimination diagrams (for example, [2, 82]). However, these diagrams could not be applied in this study due to the absence of Na_2O among the major oxides. Instead, we applied the diagrams of Fe_2O_3+MgO vs TiO_2 and Al_2O_3/SiO_2 [82] (Fig. 14). These discrimination diagrams effectively differentiate the tectonic settings into four distinct zones: oceanic island arc, continental island arc, active continental margin, and passive margin. In this study, the shales were grouped near the continental island arc on the plot of Fe_2O_3+MgO vs TiO_2 (Fig. 14a) while they were grouped near the passive margin on the plot of Fe_2O_3+MgO vs Al_2O_3/SiO_2 (Fig. 14b).

ISSN 0795 - 22066

STATISTICAL ANALYSES

Factor analysis, Hierarchical Cluster Analysis, and Pearson's correlation were applied to this study to enhance the results and discussion. They are discussed in the sections below:

FACTOR ANALYSIS

Factor analysis, a multivariate statistical technique, is commonly utilized as a valuable tool for examining exploration data in the field of geochemical studies. Several researchers [83, 84, 85, 86, 87, 88, 89, 90] have illustrated its effectiveness and relevance. In contrast to employing primary data, factor analysis can categorize and minimize the number of geochemical variables by factor score calculation [89]. The technique is usually employed in the field of geochemistry and mineral exploration for the analysis of geochemical data to distinguish mineralization from the surrounding background. This has been well-documented in the literature by several authors [84, 87, 89, 91, 92, 93, 94].

Factor analysis seeks to achieve principal components that are robust to the presence of outliers through the replacement of the traditional covariance matrix with the reweighed minimum covariance determinant estimator, a method introduced by Rousseeuw and Van Driessen [95]. To examine the relationship among the elemental data, factor analysis was employed in the present study. Table 5 presents the factor loading, eigenvalues, variance %, and variance cumulative %.

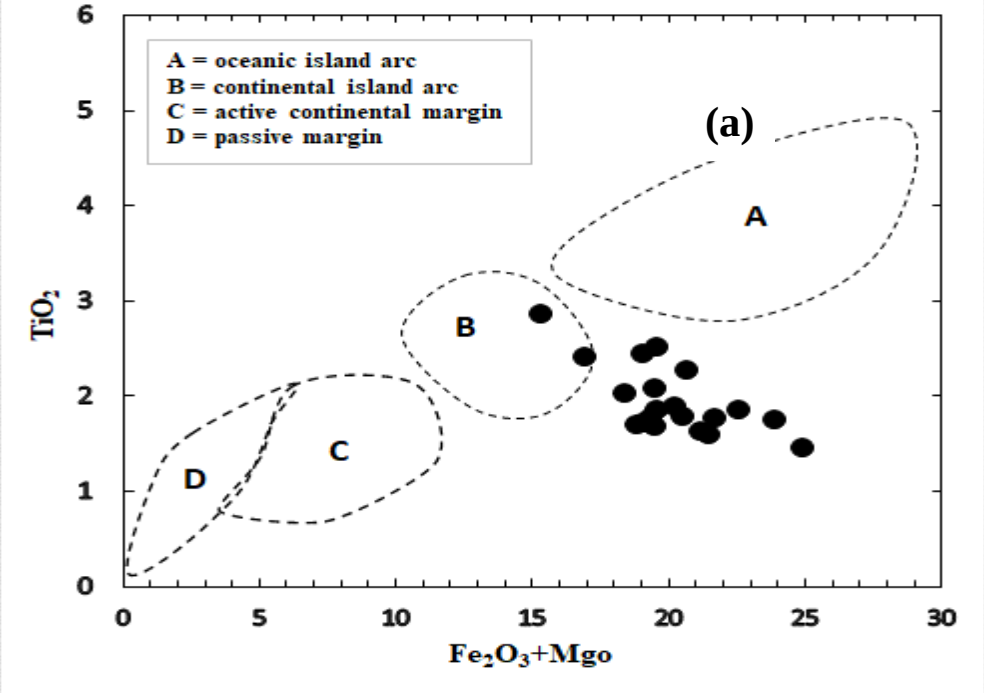

ISSN 0795 - 22066

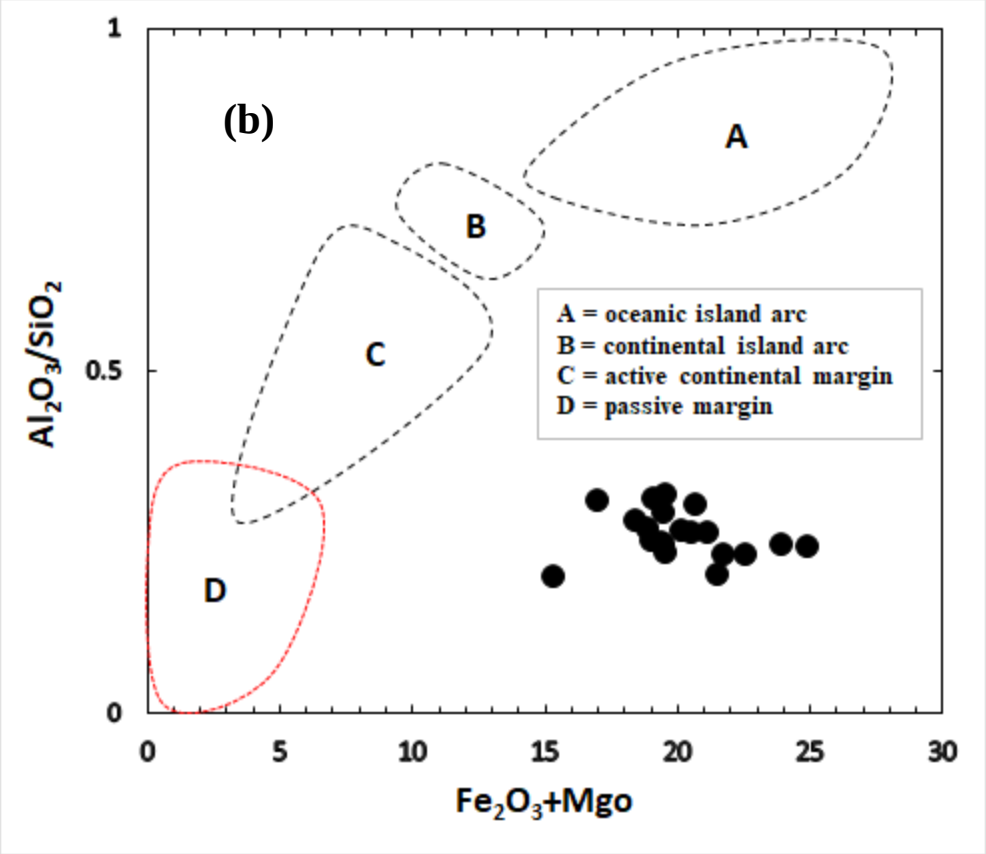

Fig. 14: Cross plots of Fe_2O_3 + MgO vs. (a) TiO_2 (after [82]) and (b) Al_2O_3/SiO_2 (after [82]) showing the tectonic settings of Gamba formation.

The 20 elements were categorized into 8 factors utilizing IBM SPSS-19.0 statistical software, which accounts for 83.18 % of the total variance and eigenvalues greater than 1 of the shales geochemical data in the subsequent groups (Table 5). The factor 1 and rotated component matrix have variance values of 19.03 % and 13.19 %, respectively (Table 5). Ba, Gd, Pr, and U were found to be associated with factor 1 and rotated component matrix which were identified as a combination of mineralization and lithology with the influence of a felsic or granitic/pegmatitic lithology in the area. The second most notable factor, accounting for 14.01 % of the model variance and rotated component matrix variance of 13.13 % (Table 5), suggests a felsic or granitic/pegmatitic lithology and sulfide mineralization in the region due to the fairly strong correlation of Bi, Mg, Nb, Th, and Ti. Factor 3 accounts for 11.64% of the variance and 11.75% rotated component variance of the eight-factor model (Table 5). The presence and influence of felsic, carbonaceous, or sulfide minerals in the area are suggested by the fairly positive correlation of Ce, Eu, Gd, and Zn. Factor 4,

ISSN 0795 - 22066

which is considered a mineralization factor due to the presence of mafic lithology, accounts for 10.56% of the model variability and 10.33% of the variance of the rotated component matrix due to the presence of Eu, Nb, and Sm within the factor. Factor 5, which accounts for 9.37% of the model variability and rotated component variance of 9.30%, indicates mineralization and mafic lithology through the occurrence of weak association of K, Nd, and Nb within the factor. Factor 6 has 7.46 % of the model variability and rotated component matrix variance of 8.73 %, suggesting felsic and mafic lithology through the occurrence of weak association of K, Nd, and Sr within the factor. Factor 7 has 5.85 % of the model variability and rotated component variance of 8.47 %, suggesting mineralization and lithology with the influence of felsic or carbonaceous mineralization in the area through the occurrence of weak association of Ca, Hf, Ta, and U within the factor. Factor 8, which accounts for 5.26% of the model variability and rotated component variance of 8.28%, indicates mineralization and mafic lithology through the occurrence of weak association of Hf, Ta, Th, and U within the factor.

HIERARCHICAL CLUSTER ANALYSIS

A statistical examination was employed to assess the shales according to their elemental composition to ascertain their degree of resemblance or divergence through the application of cluster analysis, which serves as a beneficial method for distinguishing unique groupings of earth sciences materials [96]. The hierarchical cluster analysis (Fig. 15) using the Ward technique and Euclidean distance showed three clusters of the elements. The first includes Eu, Hf, Ce, Ta, U, Nb, Nd, Gd, Zn, Bi, Ti, Sm, Sr, Pr, Ba, and Th; the second cluster includes Zn, K, Mg, and Na whereas the third cluster includes K, Mg, Na, and Ca. This cluster analysis further supports that the Gamba shales are composed of mixed provenances already inferred from the factor analysis. Furthermore, the first cluster revealed the influence of Th on the distribution of Eu, Hf, Ce, Ta, U, Nb, Nd, and Gd, the second revealed the influence of Na on Zn whereas the third revealed the influence of K, Mg, and Na on Zn.

ISSN 0795 - 22066

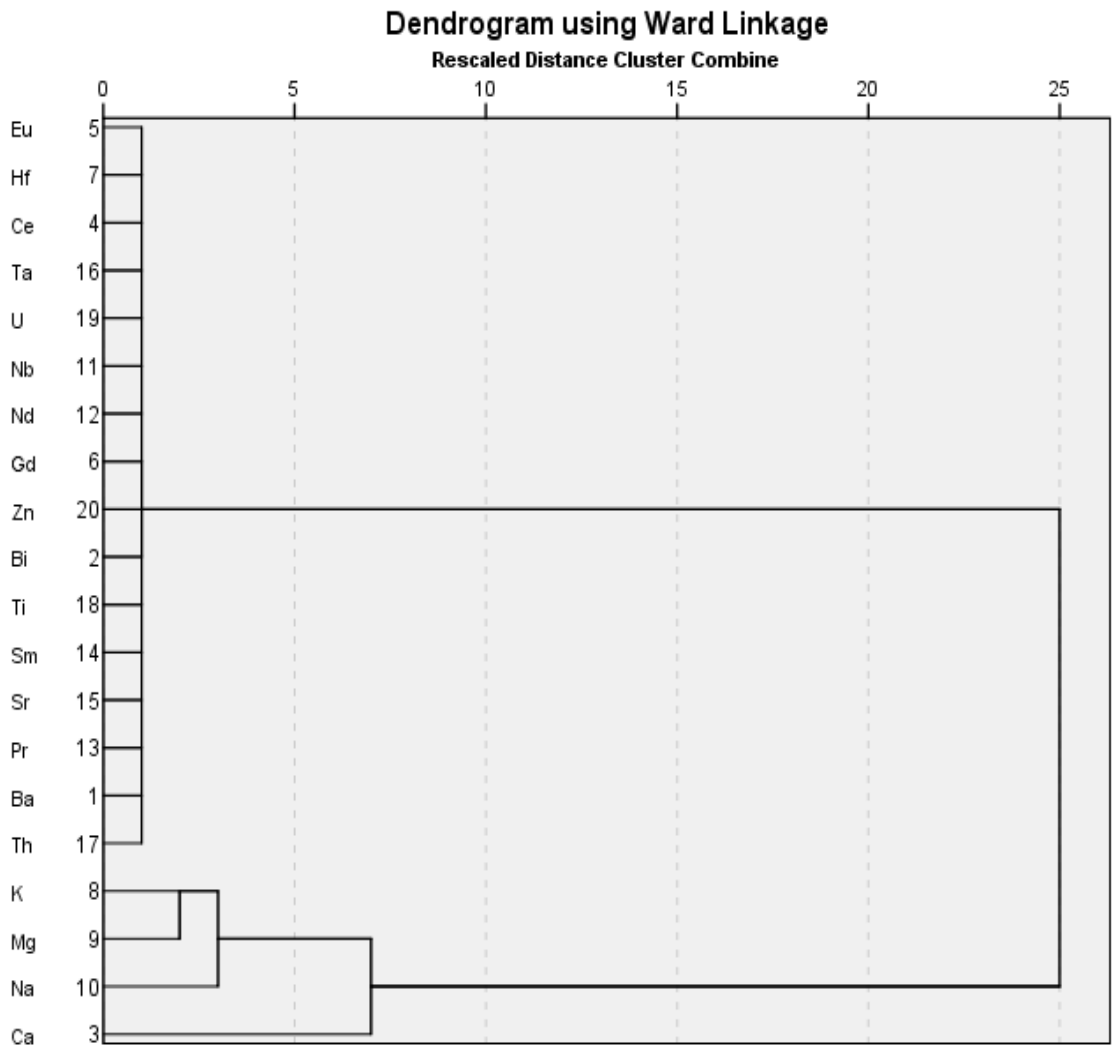

Fig. 15: The dendrogram of the cluster analysis of the shale samples from Gamba formation showing three groups of elements in the shales.

ISSN 0795 - 22066

Table 5: Results of the factor analysis of the elements

Component Matrix									Rotated Component Matrix								
Variables	PC1	PC2	PC3	PC4	PC5	PC6	PC7	PC8	**Variables**	PC1	PC2	PC3	PC4	PC5	PC6	PC7	PC8
Ba	**0.71**	0.39	0.38	-0.04	-0.08	0.18	0.25	0.03	**Ba**	0.85	-0.06	0.21	-0.24	-0.20	0.01	0.18	0.04
Bi	-0.63	0.38	0.21	0.33	0.06	0.11	0.07	0.22	**Bi**	-0.10	**0.84**	-0.07	0.07	0.03	0.03	-0.15	-0.10
Ca	0.46	0.18	-0.28	-0.04	-0.30	0.39	-0.40	0.39	**Ca**	0.10	-0.12	0.08	-0.11	0.05	0.31	**0.82**	-0.22
Ce	-0.43	0.05	**0.66**	-0.26	-0.27	-0.07	0.09	0.28	**Ce**	-0.13	0.51	0.02	-0.62	-0.23	-0.34	-0.10	0.12
Eu	0.05	-0.23	0.29	**0.60**	0.53	-0.08	0.08	0.16	**Eu**	0.11	0.23	**0.65**	0.36	0.29	-0.18	-0.29	0.01
Gd	**0.82**	0.14	0.24	0.08	0.10	-0.18	-0.22	0.27	**Gd**	0.47	-0.28	**0.60**	-0.01	-0.26	-0.08	0.33	-0.26
Hf	-0.24	-0.57	0.01	0.20	-0.37	0.18	**0.41**	0.05	**Hf**	-0.29	0.1	0.07	-0.11	0.24	0.09	-0.04	**0.76**
K	-0.04	-0.45	-0.15	-0.20	0.27	**0.60**	0.13	0.042	**K**	0.001	-0.15	-0.15	-0.1	**0.77**	-0.14	0.11	0.17
Mg	-0.43	**0.69**	-0.05	0.25	-0.21	0.03	0.34	-0.09	**Mg**	0.17	**0.66**	-0.43	0.18	-0.30	0.31	-0.14	0.07
Na	-0.36	0.31	0.14	-0.68	0.18	0.08	0.35	0.07	**Na**	0.21	0.25	-0.64	-0.27	-0.01	-0.52	-0.08	-0.04
Nb	-0.04	**0.62**	-0.40	0.06	**0.40**	-0.24	0.16	0.11	**Nb**	0.28	0.21	-0.33	**0.64**	-0.21	-0.14	0.06	-0.31
Nd	-0.18	-0.38	-0.02	0.21	**0.46**	**0.57**	-0.01	-0.002	**Nd**	-0.05	0.1	0.10	0.08	**0.85**	-0.00	-0.11	-0.003
Pr	**0.57**	0.43	0.05	0.001	0.43	0.27	0.27	-0.02	**Pr**	**0.86**	-0.06	0.01	0.18	0.14	-0.03	0.09	-0.17
Sm	-0.04	-0.03	-0.51	**0.57**	0.23	-0.30	0.11	0.13	**Sm**	-0.16	0.07	0.16	0.83	-0.01	0.08	0.01	0.10
Sr	0.03	0.34	-0.24	0.47	-0.58	0.28	-0.03	-0.29	**Sr**	0.04	0.16	-0.12	0.06	-0.15	**0.89**	0.12	0.13
Ta	0.30	0.10	-0.48	-0.18	-0.21	0.11	0.23	**0.55**	**Ta**	0.14	-0.06	-0.19	0.20	-0.06	-0.18	**0.77**	0.24
Th	-0.60	-0.08	0.04	0.35	-0.19	0.05	-0.06	**0.46**	**Th**	-0.50	**0.66**	0.12	0.04	0.08	0.01	0.15	0.14
Ti	-0.07	**0.58**	0.48	0.31	0.07	0.43	-0.26	-0.11	**Ti**	0.36	0.54	0.14	-0.27	0.09	0.41	-0.15	-0.47
U	**0.68**	-0.22	-0.12	0.23	-0.29	0.05	**0.43**	-0.11	**U**	0.41	-0.41	0.25	0.12	-0.07	0.28	0.16	**0.58**
Zn	0.44	-0.31	**0.69**	0.28	-0.12	-0.18	0.18	0.10	**Zn**	0.27	-0.04	0.77	-0.29	-0.17	-0.1	-0.16	0.34
% VAR	19.03	14.01	11.64	10.56	9.37	7.46	5.85	5.26	**% VAR**	13.19	13.13	11.75	10.33	9.30	8.73	8.47	8.28
% CVAR	19.03	33.05	44.68	55.24	64.61	72.06	77.91	83.17	**% CVAR**	13.19	26.32	38.07	48.40	57.69	66.42	74.89	83.17
EV	3.81	2.80	2.33	2.11	1.88	1.49	1.17	1.05	**EV**	2.64	2.63	2.35	2.07	1.86	1.75	1.69	1.66

N. B. EV=Eigen value, VAR= explained variance, CVAR=cumulative variance explained.

ISSN 0795 - 22066

CONCLUSIONS

The concentrations of alkali metals and alkali-earth metal elements such as Na, K, Ca, and Mg were found to be enriched in the shale samples. On the other hand, uranium (U) exhibited depleted values, suggesting that the detritus originated from diverse provenances including felsic and mafic sources under reducing environmental conditions. The shales revealed the presence of various rare earth elements, with a notable enrichment of light rare earth elements in comparison to heavy rare earth elements, suggesting the prevalence of anoxic conditions. Among the major oxides detected, SiO_2 has the highest concentration, followed by Fe_2O_3 > Al_2O_3 while most others had low values, implying shales composed principally of quartz minerals and deposited in marine environments. Additionally, the elements and oxides showed similar distribution patterns on the spider diagrams of UCC and PAAS. The ratios computed from the elements and major oxides and discrimination diagrams suggested that the shales are composed of mafic and felsic detritus and deposited under mixed conditions (anoxic and oxic) but with higher contribution from anoxic conditions near the passive margin and continental island arc. These inferences were supported by the multivariate statistical analyses performed on the elemental data. The investigation demonstrated that the geochemical analysis of trace elements and major oxides proved to be a valuable method for assessing the origin, tectonic conditions, and palaeoenvironmental settings of shale deposits.

ACKNOWLEDGMENTS

The authors appreciate the anonymous reviewers and editors of this work whose thorough reviews have improved the quality of this paper.

FUNDING

This work received no funding from any source

CONFLICT OF INTERESTS

The authors declare that they have no conflict of interest.

REFERENCES

1. Nesbitt HW, Young GM. Early Proterozoic climates and plate motions inferred from major element chemistry of lutites. Nature 1982; 299:715–717.

2. Roser BP, Korsch RJ. Determination of tectonic setting of sandstone-mudstone suites using SiO_2 content and K_2O/Na_2O ratio. J. Geol. 1986; 94:635–650.

3. Condie KC, Wronkiewicz DJ. The Cr/Th ratio in Precambrian pelites from the Kaapvaal Craton as an index of craton evolution. Earth Planet. Sci. Lett. 1990; 97:256–267.

ISSN 0795 - 22066

4. Hayashi KI, Fujisawa H, Holland HD, Ohmoto H. Geochemistry of ~1.9 Ga sedimentary rocks from northeastern Labrador, Canada. Geochem. Cosmochim. Acta
1997; 61:4115–4137.

5. Cullers RL. The controls on the major and trace element variation of shales, siltstones, and sandstones of Pennsylvanian-Permian age from uplifted continental blocks in
Colorado to platform sediment in Kansas, USA. Geochem. Cosmochim. Acta 1994; 58:4955–4972.

6. Tribovillard N, Algeo TJ, Lyons T, Riboulleau A. Trace metals as paleo-redox and
paleo-productivity proxies: An update: Chemical Geology 2006: 232:12-32.

7. Ghosh S, Sarkar S. Geochemistry of Permo-Triassic mudstone of the Satpura Gondwana basin, central India: Clues for provenance. Chem. Geol. 2010; 277:78–100.

8. Zhou L, Friis H, Poulsen MLK. Geochemical evaluation of the late Paleoceneand early
Eocene shales in Siri Canyon, Danish-Norwegian basin. Mar. Pet. Geol. 2015; 61:111–
122.

9. Toyin A, Adekeye OA. Assessment of Chemical and Mineralogical composition of Tertiary Shales from the Nigerian sector of Iullemmeden basin: Implication for Paleoclimate and Provenance. J. Afr. Ear. Sci. 2018; doi: 10.1016/j.jafrearsci.2018.09.006

10. Li H, Liu B, Liu X, Meng L, Cheng L, Wang H. Mineralogy and inorganic geochemistry of the Es4shales of the Damintun Sag, northeast of the Bohai Bay basin: Implication for depositional environment. Mar. Petr. Geol. 2019; 110:886–900.

11. Li G, Qin Y, Shen J. Geochemical characteristics of the Upper Paleozoic coal series
shale in the Linxing area, Ordos Basin, China: implications for paleoenvironment, provenance, and tectonic setting, Arabian Journal of Geosciences 2021; 14 (3):
10.1007/s12517-021-06470-3.

12. Asjad S., Ahmad AHM, Quasim MA, Sachan HK. Provenance, palaeoweathering and tectonic setting of the Kuldhar Member Shale (Callovian–Oxfordian), Jaisalmer
Formation, western Rajasthan. *J. Sediment. Environ.* 2021; **6**:585–602.

13. Quasim MA, Absar N, Singh BP, Ahmad F., Murugan A. Geochemistry of
Mesoproterozoic Bijaigarh Shale, Upper Vindhyan Group, Son Valley, India:
Implications for source area weathering, provenance and tectonic setting. *J Earth Syst Sci* 2023; **132**:115.

14. Ogbesejana AB, Dairu FR, Nasiru SG, Aminu LM, Okunola OJ, Bello OM.
Elemental Geochemistry of the Late Paleocene Shales from Dange and Gamba
Formations, Sokoto basin, Northwest Nigeria. Nig. Res. J. Chem. Sci. 2024; 12 (1): 23-50.

15. McLennan SM. Rare earth elements in sedimentary rocks: influence of provenance and sedimentary processes. Rev. Mineral. Geochem. 1989; 21:169–200.

16. Li Q, Wu S, Xia D, You X, Zhang H, Lu H. Major and trace element geochemistry of
the lacustrine organic-rich shales from the Upper Triassic Chang 7 Member in the
southwestern Ordos Basin, China: Implications for paleoenvironment and organic
matter accumulation. Mar. and Petr. Geol. 2020; 111: 852-867.

17. Ming X, Li X, Zhang Q, Guo H, Zhang Z, Cao Y, Shen J, Zhang C. Provenance,

ISSN 0795 - 22066

chemical weathering, and sedimentary environment of the aquifer sediments:
Implication for arsenic enrichment in groundwater. Cat. 2024; 239:107915.

18. Qi L, Wang H, Hi Z, Zhou T, Li G, Sun S, Cheng F. Mineralogical and Geochemical
Characteristics of the Deeply Buried Wufeng–Longmaxi Shale in the Southern
Sichuan Basin, China: Implications for Provenance and Tectonic Setting, Minerals
2023;13(12):1502.

19. Liu B, Song Y, Zhu K, Su P, Ye X, Zhao W. Mineralogy and element geochemistry
of salinized lacustrine organic-rich shale in the Middle Permian Santanghu basin:
Implications for paleoenvironment, provenance, tectonic setting and shale oil
potential. Mar. and Petr. Geol. 2020; 120:104569.

20. Cox R, Lowe DR, Culler RL. The influence of sediment recycling and basement
composition on evolution of mudrock chemistry in the southwestern United States.
Geochem. Cosmochim. Acta 1995; 59:2919–2940.

21. Tao S, Shan Y, Tang D, Xu H, Li S, Cui Y. Mineralogy, major and
trace element geochemistry of Shichanggou oil shales, Jimusaer, Southern Junggar
basin, China: implications for provenance, palaeoenvironment and tectonic
setting. J. Pet. Sci. Eng. 2016; 146:432–445.

22. Zhang S, Liu C, Liang H, Wang J, Bai J, Yang M, Liu G, Huang H, Guan Y.
Paleoenvironmental conditions, organic matter accumulation, and unconventional
hydrocarbon potential for the Permian Lucaogou Formation organic-rich rocks in
Santanghu basin, NW China. Int. J. Coal Geol. 2018; 185:44–60.

23. Zhang W, Yang W, Xie L. Controls on organic matter accumulation in the
Triassic Chang 7 lacustrine shale of the Ordos basin, central China. Int. J. Coal
Geol. 2017; 183:38–51.

24. Kogbe CA. Cretaceous and Tertiary of the Iullemmeden basin in Nigeria (West
Africa). Cret. Res. 1981; 2:129 – 186.

25. Kogbe CA. Geology of the south-eastern (Sokoto) sector of the Iullemmeden basin.
Bulletin Department of Geology, Ahmadu Bello University, Zaria, Nigeria 1979a; 2
(1): xv + 420.

26. Kogbe CA. Outline of the Geology of the Iullemmeden basin in North– western
Nigeria. In: Geology of Nigeria (Edited by Kogbe, C. A) 1976; 331 – 338 Elizabethan
Pub. Co., Lagos, Nigeria.

27. Obaje NG. Foraminiferal biostratigraphy and paleoenvironment of the Sokoto Basin
of NW Nigeria. M.Sc Thesis, Ahmadu Bello University, Zaria. 1987; 76pp

28. Obaje NG. Geology and Mineral Resources of Nigeria. Springer, Heildelberg 2009;
221pp.

29. Obaje NG, Wehner H, Scheeder G, Abubakar MB, Jauro A. Hydrocarbon
prospectivity of Nigeria's inland basins: From the viewpoint of organic geochemistry
and organic petrology. American Association of Petroleum Geologists Bulletine 2004;
87:325-353.

30. Obaje NG, Adukub M, Yusuf I. The Sokoto Basin of Northwestern Nigeria: A
Preliminary Assessment of the Hydrocarbon Prospectivity. Petr. Tech. Dev. J. 2013; 3
(2):66-80.

31. Toyin A, Sanni ZJ, Adekeye OA, Bale RB, Jimoh O.A. Lithostratigraphic

ISSN 0795 - 22066

Description, Sedimentology and Depositional Environment of Rocks Penetrated by
Illela Borehole, Sokoto basin, NW Nigeria: A connection between Gulf of Guinea
basins. J. Afr. Ear. Sci. 2016; 121:255-266.

32. Emujakporue G, Ofoha CC, Kiani I. Investigation into the basement morphology and
tectonic lineament using aeromagnetic anomalies of Parts of Sokoto Basin, North
Western, Nigeria. Egy. J. Petr. 2018; 27(4):671-681.

33. Toyin A, Adekeye OA, Bale RB, Sanni ZJ. Carbonate Sedimentology and
Depositional Environment of Carbonate Rocks of the Kalambaina Formation,
Penetrated by Illela Borehole, Sokoto basin, NW Nigeria. Nig. Min. Geo. Soc
(NMGS) J. 2015; 51(1):47-55.

34. Reyment RA. The ostracoda of the Kalambaina (Paleocene) northwest Nigeria. Bull.
Geol. Inst. Univ. of Uppsala 1981; 5(9):57-65.

35. Bassey C, Eminue O. Preliminary evaluation of major and trace elements content ofCretaceous – Palaeogene Formation of the Sokoto Basin, Northwestern Nigeria.
NAFTA 2014; 65(1):69-76.

36. Boboye OA, Adeyemi MS, Madukwe HY. Lithostratigraphy and Inorganic Geochemical Studies of Cretaceous-Tertiary Lithofacies from Nigerian Three Inland Basin. Open J. Geol. 2018; 8:711-736.

37. Petters SW. Stratigraphical history of the south-central Sahara region. Bull. Geol. Soc.
Amer. 1979a; 90:753-760.

38. Jones B. The sedimentary rocks of Sokoto province. Bull.Geol. Surv. Nig. 19; 18.

39. Petters SW. Foraminiferal Paleoecology ofthe southern part of the Maastrichtian –
Paleocene Saharan epeiric sea. J. For. Res. 1978a; 8:303-313.

40. Petters SW. Maastrichtian –Paleocene foraminifera from NW Nigeria and their
paleogeography. Acta palaeont .pol. 1978d; 23:131-152.

41. Krasheninnikov VA, Trofimov DM. Sravitel'nyy analiz benthosnykh foraminifer
datsko-paleotsenovykh otlozhneniy Mali, oblasti tetisa I severo-zapodny Evropy.
Vopr. Micropaleont. SSSR 1969; 12:108-144.

42. Greigert J. Description des formations Cretaces et Tertiaires du basin de Iullemeden.
Mem. Bur. Rech. geol.min 1966; 36.

43. Furon R. Geology of Africa. Oliver and Boyd 1963.

44. Radier H. Contribution a letude geologique du Suodan oriental (A.O.F.). Le basin Cretace et tertiaire de Gao le detroit Soudanais. Bull. Serv. geol. Prosp. Min. 1959;
26:315-556.

45. Kogbe CA. Geology of the Upper Cretaceous and Tertiary sediments of the Nigerian
sector of the Iullemeden basin (West Africa). Geol. Rdsch. 1973; 62:197-211.

46. Liu CW, Lin KH, Kuo YM. Application of factor analysis in the assessment of
ground water quality in the Blackfoot disease area in Taiwan. Sci. Tot. Env. 2003;
313:77–89.

47. Massart DL, Vandeginste BGM, Deming SN, Michotte Y, Kaufman L. Chemometrics, A Textbook. Amsterdam: Elsevier. 1988.

48. Helena BA, Vega M, Barrado E, Pardo R, Fernandez L. A Case of Hydrochemical
Characterization of an Alluvial Aquifer Influenced by Human Activities. Water Air
Soil Pollut. 1999; 112:365–387.

ISSN 0795 - 22066

49. Willet P. Similarity and Clustering in Chemical Information Systems. Chichester: Wiley, Research Studies Press 1987.

50. Gromet LP, Haskin LA, Korotev RL, Dymek RF. The"North American shale composite": its compilation, major and trace element characteristics. Geochim Cosmochim Acta 1984; 48:2469–2482.

51. Käpyaho A, Arslan M, Carbone S, Nykänen V. Rare Earth Elements as Indicators of Petroleum Generation Potential in Shale Formations. Minerals 2019; 9(5):290.

52. Klein C, Hurlbut CS. Manual of mineralogy. John Wiley & Sons, New York 1993.

53. Elderfield H, Greaves MJ. The rare earth elements in seawater. Nature 1982; 296:214–219.

54. de Baar HJ, German CR, Elderfield H, Van Gaans P. Rare earth element distributions in anoxic waters of the Cariaco Trench. Geochem. Cosmochim. Acta 1988; 52(5):1203–1219.

55. Taylor SR, McLennan SM. The Continental Crust: Its Composition and Evolution, Blackwell Publishing, Oxford, UK 1985.

56. Niu YL, Liu Y, Xue QQ, Shao FL, Chen S, Duan M, Guo PY, Gong HM, Hu Y, Hu ZX, Kong JJ, Li JY, Liu JJ, Sun P, Sun WL, Ye L, Xiao YY, Zhang Y. Exotic origin of the Chinese continental shelf: New insights into the tectonic evolution of the western Pacific and eastern China since the Mesozoic. Sci. Bull. 2015; 60:1598-1616.

57. Yang JH, Du YS. Weathering geochemistry and palaeoclimate implication of the Early Permian mudstones from eastern Henan Province, North China. J. Palaeogeography 2017; 6(4):370-380.

58. Edema AA, Olatunji AS Bamidele O. Inorganic Geochemical Evaluation and Aspects of Rock Eval Pyrolysis of Eocene to Recent Sediments of Soso and Kay-1 Wells, Western Niger Delta, Nigeria. J. Env. Ear. Sci. 2016; 6 (10): 67-90.

59. Pundaree N, Keshav Krishna A, Subramanyam KSV, Sawant SS, Kavitha S, Kalpana MS, Patil DJ, Dayal AM. Early Eocene carbonaceous shales of Tadkeshwar Formation, Cambay basin, Gujarat, India: Geochemical implications, petrogenesis and tectonics, Marine and Petroleum Geology 2015;

http://dx.doi.org/10.1016/j.marpetgeo.2015.08.028

60. Federman AN, Grotzinger JP, Milliken RE. Mineralogy and sedimentology of a sulfate-rich outcrop of the Burns Formation (MER) on the plains of Gusev crater, Mars. J. Geophy. Res: Planets 1999; 104(E4):8673-8715.

61. Akinyemi SA, Adebayo OF, Madukwe HY, Kayode AT, Aturamu AO, OlaOlorun OA, Nyakuma BB, Jauro A, Gitari WM, Mudzielwana R, Hower JC. Elemental geochemistry and organic facies of selected Cretaceous coals from the Benue Trough basin in Nigeria: Implication for paleodepositional environments. Mar. Petr. Geol. 022; 137:105490.

62. Holland HD. The Chemical Evolution of the Atmosphere and Oceans. Princeton University Press 1984.

63. Jones B, Manning AC. Comparison of geochemical indices used for the interpretation of palaeoredox conditions in ancient mudstones. Chem. Geol. 1994;111:111–129.

64. Zhang K, Liu R, Liu Z, Li B, Han J, Zhao K. Influence of volcanic and hydrothermal activity on organic matter enrichment in the Upper Triassic Yanchang Formation,

ISSN 0795 - 22066

southern Ordos basin, Central China. Mar. Petrol. Geol. 2020; 112: 104059.

65. Wignall PB, Twitchett RJ. Oceanic anoxia and the end Permian mass extinction. Sci. 1996; 272 (5265):1155–1158.

66. Wignall PB, Myers KJ. Interpreting benthic oxygen levels in mudrocks: a new approach. Geol. 1988; 16(5):452–455.

67. Aihua W. Discriminant effect of sedimentary environment by the Sr/Ba ratio of different exising forms [J]. Acta Sedimentol. Sin. 1996; 4.

68. Deng HW, Qian K. Analysis on Sedimentary Geochemistry and Environment. Gansu Sci. Tech. Pub. House, Lanzhou 1993.

69. Liu Y, Cao L, Li Z, Wang H, Chu T, Zhang J. Element Geochemistry. Science and Technology Press, Bejing ([in Chinese]) 1984.

70. Wei W, Algeo TJ, Lu Y, Lu YC, Liu H, Zhang S, Peng L, Zhang J, Chen L. Identifying marine incursions into the Paleogene Bohai Bay basin lake system in northeastern China. Int J Coal Geol. 2018; 200:1–17

71. Wei W, Algeo TJ. Elemental proxies for paleosalinity analysis of ancient shales and mudrocks. Geochem. Cosmochim. Acta 2019; https://doi.org/10.1016/j. gca.2019.06.034.

72. Demaison GJ, Moore GT. Anoxic environments and oil source bed genesis. AAPG (Am. Assoc. Pet. Geol.) Bull. 1980; 64(8):1179–1209.

73. Hurowitz JA, McLennan SM. Geochemistry of Cambro-Ordovician sedimentary rocks of the northeastern United States. Changes in sediment sources at the onset of Taconian orogenesis,"J. Geol. 2005;113(5):571–587.

74. McLennan,S.M., Hemming, S., McDaniel, D.K., Hanson, G.N., 1993. Geochemical approaches to sedimentation, provenance and tectonics," in Processes Controlling the Composition of Clastic Sediments, MJ Johnsson and A. Basu, Eds., Geological Society of America Special Paper 1993; 284:21–40.

75. Gu XX, Liu JM, Zheng MH, Tang JX, Qi L. Provenance and Tectonic Setting of the Proterozoic Turbidites in Hunan, South China: Geochemical Evidence. J. Sed. Res. 2002; 72 (3): 393–407.

76. Rudnick RL. Restites, Euanomalies and the lower continental crust,"Geochimica et Cosmochimica Acta 1992; 56(3):963–970.

77. Oni SO, Olatunji AS, Ehinola OA. Determination of Provenance and Tectonic Settings of Niger Delta Clastic Facies Using Well-Y, Onshore Delta State, Nigeria. J. Geochem. 2014; 1-13.

78. Wakita H, Rey P, Schmitt RA. Abundances of the 14 rare-earth elements and 12 other trace elements in Apollo 12 samples: Five igneous and one breccia rocks and four soils," in Proceedings of the Second Lunar Science Conference 1971; 1319–1329, Pergamon Press, Oxford, UK.

79. Cullers RL. The geochemistry of shales, siltstones and sandstones of Pennsylvanian-Permian age, Colorado, USA: implications for provenance and metamorphic studies,"Lithos 2000; 51(3):181–203.

80. Harnois L.The CIW index: a new chemical index of weathering. Sediment. Geol. 1988; 55:319–322.

81. Middleburg JB, Van der Weijden CH, Woittiez JRW. Chemical processes affecting the mobility of major, minor and trace elements during weathering of granitic rocks. Chem. Geol. 1988; 68:253–273.

ISSN 0795 - 22066

82. Bhatia MR. Plate tectonics and geochemical composition of sandstones: Journal of Geology,Volume 1983; 91:611-627.

83. Borovec Z. Evaluation of the concentrations of trace elements in stream sediments by factor and cluster analysis and the sequential extraction procedure. Sci Total Environ 1996; 177:237–250.

84. Helvoort PJ, Filzmoser P, Gaans PFM. Sequential factor analysis as a new approach to multivariate analysis of heterogeneous geo-chemical datasets: an application to a bulk chemical characterization of fluvial deposits (Rhine–Meuse delta, The Netherlands). Appl. Geochem. 2005; 20:2233–2251.

85. Kumru, M.N., Bakac, M. R-mode factor analysis applied to the distribution of elements in soils from the Aydın basin, Turkey. J Geochem Explor 2003; 77:81–91.

86. Reimann C, Filzmoser P, Garrett RG. Factor analysis applied to regional geochemical data: problems and possibilities. Appl Geochem 2002; 17:185–206.

87. Shamseddin Meigoony, M., Afzal, P., Gholinejad, M., Yasrebi, A.B.,, Sadeghi, B. Delineation of geochemical anomalies using factor analy-sis and multifractal modeling based on stream sediments data in Sarajeh 1:100,000 sheet, Central Iran. Arab J Geosci. 2013; doi:10.1007/s12517-013-1074-3

88. Sun, X., Deng, J., Gong, Q., Wang, Q., Yang, L., Zhao, Z. Kohonen neural network and factor analysis based approach to geochemical data pattern recognition. J Geochem Explor 2009; 103:6–16.

89. Yousefi, M., Kamkar-Rouhani, A., Carranza, E.J.M. Geochemical mineralization probability index (GMPI): a new approach to gener-ate enhanced stream sediment geochemical evidential map for in-creasing probability of success in mineral potential mapping. J Geochem Explor 2012; 115:24–35.

90. Yousefi, M., Kamkar-Rouhani, A., Carranza, E.J.M. Application of staged factor analysis and logistic function to create a fuzzy stream sediment geochemical evidence layer formineral prospectivity mapping. Geochem Explor Environ Anal 2014; 14:45–58.

91. Muller J, Kylander M, Martinez-Cortizas A, Wüst RAJ, Weiss D, Blake K, Coles B, Garcia-Sanchez R. The use of principle compo-nent analyses in characterizing trace and major elemental distribu-tion in a 55 kyr peat deposit in tropical Australia: implications to paleoclimate. Geochim Cosmochim Acta 2008; 72:449–463.

92. Zuo, R. Identifying geochemical anomalies associated with Cu and Pb–Zn skarn mineralization using principal component analysis and spectrum–area fractal modeling in the Gangdese Belt, Tibet (China). J Geochem Explor 2011a; 111:13–22.

93. Zuo, R. Decomposing of mixed pattern of arsenic using fractal model in Gangdese belt, Tibet, China. Appl Geochem 2011b; 26:S271–S273.

94. Zuo R, Cheng Q, Xia Q. Application of fractal models to character-ization of vertical distribution of geochemical element concentration. J Geochem Explor 2009; 102:37–43.

95. Rousseeuw P, Van Driessen K. A fast algorithm for the minimum covariance determinant estimator. Technometrics 1999; 41(3):212–223.

96. Akinlua, A., Sigedle, A., Buthelezi, T., Fadipe, O.A. Trace element geochemistry of crude oils and condensates from South African basins. Marine and Petroleum Geology 2015; 59:286–293.

ISSN 0795 - 22066